

# First-principle Wannier functions and effective lattice fermion models for narrow-band compounds

I. V. Solovyev

PRESTO, Japan Science and Technology Agency,  
Institute for Solid State Physics, University of Tokyo,  
Kashiwanoha, Kashiwa, Chiba, 277-8581, Japan

(dated: March 23, 2024)

We propose a systematic procedure for constructing effective lattice fermion models for narrow-band compounds on the basis of first-principles electronic-structure calculations. The method is illustrated for the series of transition-metal (TM) oxides:  $\text{SrVO}_3$ ,  $\text{YTiO}_3$ ,  $\text{V}_2\text{O}_3$ , and  $\text{Y}_2\text{M}_2\text{O}_7$ , whose low-energy properties are linked exclusively to the electronic structure of an isolated  $t_{2g}$  band. The method consists of three parts, starting from the electronic structure in the local-density approximation (LDA). (i) construction of the kinetic-energy Hamiltonian using formal downfolding method. It allows to describe the band structure close to the Fermi level in terms of a limited number of (unknown yet) Wannier functions (WFs), and eliminate the rest of the basis states. (ii) solution of an inverse problem and construction of WFs for the given kinetic-energy Hamiltonian. Here, we closely follow the construction of the basis functions in the linear-muffin-tin-orbital (LMTO) method, and enforce the orthogonality of WFs to other band. In this approach, one can easily control the contributions of the kinetic energy to the WFs. (iii) calculation of screened Coulomb interactions in the basis of auxiliary WFs. The latter are defined as the WFs for which the kinetic-energy term is set to be zero. Meanwhile, the hybridization between TM  $d$  and other atomic states is well preserved by the orthogonality condition to other bands. The use of auxiliary WFs is necessary in order to avoid the double counting of the kinetic-energy term, which is included explicitly in the model Hamiltonian. In order to calculate the screened Coulomb interactions we employed a hybrid approach. First, we evaluate the screening caused by the change of occupation numbers and the relaxation of the LMTO basis functions, using the conventional constraint-LDA approach, where all matrix elements of hybridization connecting the TM  $d$  orbitals and other orbitals are set to be zero. Then, we switch on the hybridization and evaluate the screening of on-site Coulomb interactions associated with the change of this hybridization in the random-phase approximation. The second channel of screening appears to be very important, and results in relatively small value of the effective Coulomb interaction for isolated  $t_{2g}$  bands (about 2-3 eV, depending on the material). We discuss details of this screening and consider its band-filling dependence, frequency dependence, influence of the lattice distortion, proximity of other bands, as well as the effect of dimensionality of the model Hamiltonian.

PACS numbers: 71.10.Fd; 71.15.Mb; 71.28.+d; 71.15.Ap

## I. INTRODUCTION

Many successes of modern solid-state physics and chemistry are related with the development of the Hohenberg-Kohn-Sham density-functional theory (DFT)<sup>1,2</sup> which is designed for the ground state and based on the minimization of the total energy  $E[\rho]$  with respect to the electron density  $\rho$ . For practical applications, DFT resorts to iterative solution of single-particle Kohn-Sham (KS) equations,

$$\frac{\hbar^2}{2m} \nabla^2 \psi_i + V_H + V_{XC} + V_{\text{ext}} \psi_i = \epsilon_i \psi_i; \quad (1)$$

together with the equation for the electron density:

$$\rho(\mathbf{r}) = \sum_i n_i |\psi_i(\mathbf{r})|^2; \quad (2)$$

defined in terms of eigenfunctions ( $\psi_i$ ), eigenvalues ( $\epsilon_i$ ), and the occupation numbers ( $n_i$ ) of KS quasiparticles. Different terms in Eq.(1) are correspondingly the kinetic-energy operator, the Hartree potential, the exchange-correlation potential, and the external potential. In the following we will also reserve the notation  $H_{\text{KS}} = \frac{\hbar^2}{2m} \nabla^2 + V_H + V_{XC} + V_{\text{ext}}$  for the total KS Hamiltonian in the real ( $\mathbf{r}$ ) space.

The exchange-correlation potential is typically treated in the local-density approximation (LDA). It employs an analytical expression for  $V_{XC}[\rho]$  borrowed from the theory of homogeneous electron gas in which the density of the

electron gas is replaced by the local density of the real system. LDA is far from being perfect and there are many examples of so-called strongly-correlated materials for which the conventional LDA appears to be insufficient both for the excited-state and ground-state properties.<sup>3,4,5</sup>

A typical situation realized in transition-metal (TM) oxides is shown in Fig. 1. We would like to emphasize two

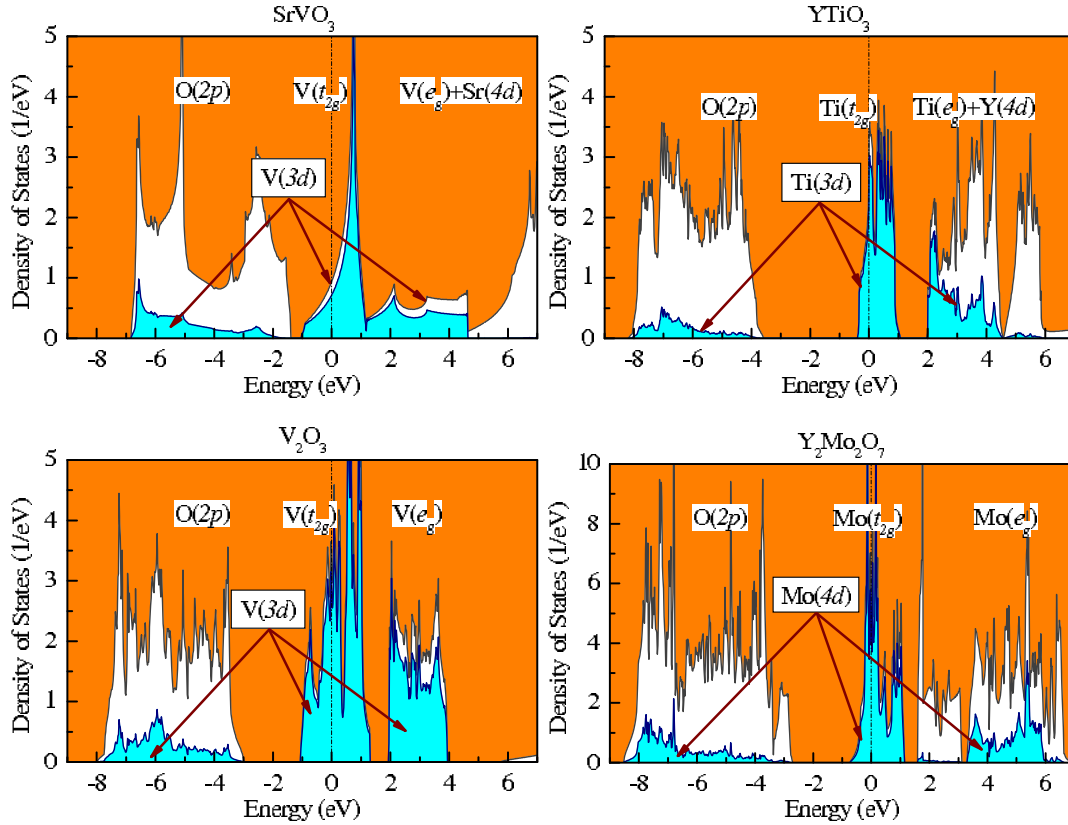


FIG. 1: Total and partial densities of states for  $\text{SrVO}_3$ ,  $\text{YTiO}_3$ ,  $\text{V}_2\text{O}_3$ , and  $\text{Y}_2\text{Mo}_2\text{O}_7$  in the local-density approximation. The shaded area shows the contributions of transition-metal d-states. Other symbols show positions of the main bands. The Fermi level is at zero energy.

points.

(i) The common feature of many TM oxides is the existence of the well isolated narrow band (or the group of bands) located near the Fermi level and well isolated from the rest of electronic states. For compounds shown in Fig. 1, this is the TM  $t_{2g}$  band, which is sandwiched between O(2p) band (from below) and a group of bands (from above), which have an appreciable weight of the TM  $e_g$  states (the meaning of many notations will become clear in Sec. VI, where we will discuss details of the crystal and electronic structure for the considered oxide compounds). Electronic and magnetic properties of these compounds are predetermined mainly by the behavior of this  $t_{2g}$  band. The effect of other bands can be included indirectly, through the renormalization of interaction parameters in the  $t_{2g}$  band.

(ii) The LDA description appears to be especially bad for the  $t_{2g}$  states located near the Fermi level. It often fails to reproduce the insulating behavior of these compounds, as well as the correct magnetic ground state, which is directly related with the existence of the band gap.<sup>6</sup> The source of the problem is known to be the on-site Coulomb correlations, whose form is greatly oversimplified in the model of homogeneous electron gas. Therefore, the basic strategy which was intensively pursued already for more than decade was to incorporate the physics of on-site Coulomb correlations in LDA and to solve this problem using modern many-body techniques. This way of thinking gave rise to such directions as LDA+U (e.g., Refs. 3, 4, and 7) and LDA+DMFT (dynamical mean-field theory, Ref. 8).

Taking into account two above arguments, we believe that the most logical way to approach the problem of Coulomb correlations in narrow-band compounds is to divide it in two parts:

- (i) mapping of conventional electronic structure calculations onto the multi-orbital Hubbard model, and derivation of the parameters of this model from the first principles, for example starting from the simplest electronic structure in LDA;
- (ii) solution of this multi-orbital Hubbard model using modern many-body methods.<sup>9</sup>

In this paper we will discuss the first part of this project and show how results of conventional LDA calculations for the  $t_{2g}$  bands can be mapped onto the multi-orbital Hubbard model:

$$\hat{H} = \sum_{R,R^0} \sum_{\alpha,\alpha^0} h_{R,R^0}^{\alpha,\alpha^0} c_{R,\alpha}^\dagger c_{R^0,\alpha^0} + \frac{1}{2} \sum_{R,R^0} \sum_{\alpha,\alpha^0} U_{R,R^0}^{\alpha,\alpha^0} c_{R,\alpha}^\dagger c_{R,\alpha^0}^\dagger c_{R^0,\alpha} c_{R^0,\alpha^0}; \quad (3)$$

where  $c_{R,\alpha}^\dagger$  ( $c_{R,\alpha}$ ) creates (annihilates) an electron in the Wannier orbital  $W_{R,\alpha}$  of the site  $R$ , and  $\alpha$  is a joint index, incorporating all remaining (spin and orbital) degrees of freedom. The matrix  $h_{R,R^0}^{\alpha,\alpha^0}$  parameterizes the kinetic energy of electrons. The matrix elements  $h_{R,R^0}^{\alpha,\alpha^0}$  have the following meaning: the site-diagonal part ( $R = R^0$ ) describes the local level-splitting, caused by the crystal field and (or) the spin-orbit interaction, while the off-diagonal part ( $R \neq R^0$ ) stands for the transfer integrals (or the transfer interactions).  $U_{R,R^0}^{\alpha,\alpha^0} = \int d\mathbf{r} \int d\mathbf{r}^0 W^{\alpha,\alpha^0}(\mathbf{r}) W^{\alpha,\alpha^0}(\mathbf{r}) v_{\text{scr}}(\mathbf{r} - \mathbf{r}^0) W^{\alpha,\alpha^0}(\mathbf{r}^0) W^{\alpha,\alpha^0}(\mathbf{r})$  are the matrix elements of screened Coulomb interaction  $v_{\text{scr}}(\mathbf{r} - \mathbf{r}^0)$ , which are supposed to be diagonal with respect to the site indices. In principle, the off-diagonal elements can be also included into the model. However, we do not consider them in the present work. In Sec. V III we will discuss several open questions related with the definition of the intersite Coulomb interactions in LDA.

The first part of this paper will be devoted to derivation of the parameters of the kinetic energy. Then, we will explain how to construct the Wannier functions (WFs), which generate these parameters after applying to the KS Hamiltonian in the real space. The next part will be devoted to calculations of screened Coulomb interactions, using the WF formalism.

## II. THE LMTO METHOD

In this section we will briefly review the main ideas of linear-muffin-tin-orbital (LMTO) method, as they will be widely used in the subsequent sections for the construction of transfer interactions and the Wannier orbitals. The method is designed for the solution of KS equations in LDA. For the details and recent developments, the reader is referred to the activity of the O.K. Andersen group at the Max-Planck Institute in Stuttgart.<sup>10</sup>

Majority of modern electronic structure methods use some basis. The basis functions of the LMTO method,  $f_{j\mathbf{L}}^{\mathbf{L}}$  (the so-called muffin-tin orbitals {MTOs}) have many similarities with orthogonalized atomic orbitals. As we will see below, the LMTO method is very convenient for constructing the WFs, and for certain applications, the basis function of the LMTO method, from the very beginning, can be chosen as a Wannier function.

The conventional LMTO approach employs the atomic-spheres-approximation (ASA), which assumes that the whole space of the crystal can be filled by overlapping atomic spheres (Fig. 2), so that the overlap between the spheres as well as the empty spaces, which are not encircled by any spheres, can be neglected. The MTOs are constructed from solutions of KS equations inside atomic spheres (the partial waves), calculated at some energies  $E_{\mathbf{L}}$  (typically, the center of gravity of the occupied band or of the entire band),  $\epsilon_{\mathbf{L}}$ , and their energy derivatives  $\epsilon'_{\mathbf{L}}$ . In each atomic sphere, the KS potential is spherically averaged. Therefore, the solutions are proportional to the angular harmonics, which are specified by the indices  $\mathbf{L} = (l, m)$  (correspondingly, orbital and azimuthal quantum numbers). At the atomic sphere boundaries,  $f_{\mathbf{L}}^{\mathbf{L}}$  and  $f'_{\mathbf{L}}^{\mathbf{L}}$  match continuously and differentiably onto certain envelop functions. The latter are typically constructed from irregular solutions of Laplace equation, which rapidly decay in the real space (Fig. 2).

It is easy to verify that the functions  $f_{\mathbf{L}}^{\mathbf{L}}$  and  $\epsilon'_{\mathbf{L}}$  obey the following "LMTO algebra":

$$h_{\mathbf{L}\mathbf{L}} f_{\mathbf{L}}^{\mathbf{L}} = 1; \quad (4)$$

$$h_{-\mathbf{L}\mathbf{L}} f_{\mathbf{L}}^{\mathbf{L}} = h_{\mathbf{L}\mathbf{L}} \epsilon'_{-\mathbf{L}} = 0; \quad (5)$$

$$h_{-\mathbf{L}\mathbf{L}} \epsilon'_{-\mathbf{L}} = p_{\mathbf{L}}; \quad (6)$$

$$(H_{\text{KS}} - E_{\mathbf{L}}) f_{\mathbf{L}}^{\mathbf{L}} = 0; \quad (7)$$

and

$$(H_{\text{KS}} - E_{\mathbf{L}}) \epsilon'_{-\mathbf{L}} = f_{\mathbf{L}}^{\mathbf{L}}; \quad (8)$$

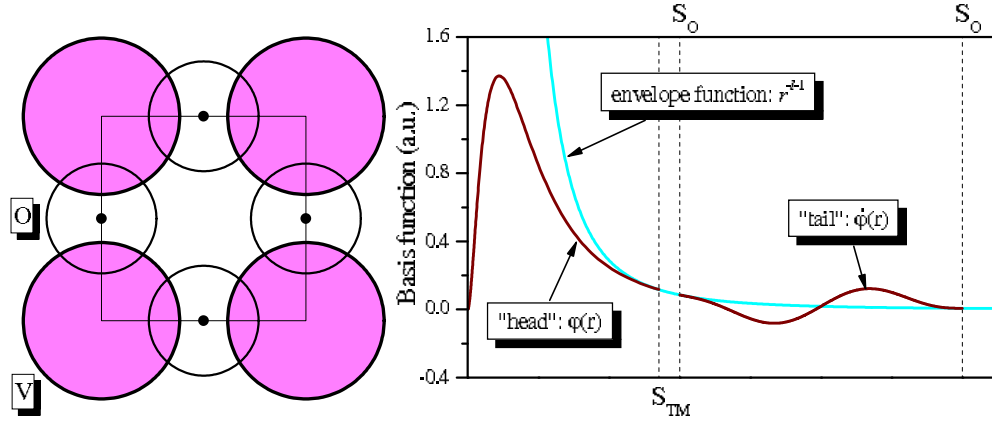


FIG. 2: Construction of basis functions of the LMTO method. It is assumed that the whole space of the crystal is filled by the atomic spheres. The left panel shows a concrete example of such filling in the  $\text{VO}_2$  plane of  $\text{SrVO}_3$ . The central part of the basis function (the "head") is constructed as the solution of Kohn-Sham equation inside atomic sphere  $R$  ( $R_L$ ), which is calculated in the center of gravity of the band and whose angular character is denoted by  $L$ . The "tail" of the basis function at the neighboring site  $R^0$  is constructed from the energy-derivatives of  $R_L^0$  (denoted as  $-R_L^0$ ). At the atomic spheres boundaries (shown by  $S_{TM}$  and  $S_0$  for the central transition-metal site and neighboring oxygen sites, respectively),  $R_L$  and  $-R_L^0$  match continuously and differentiably onto certain envelop function (typically, an irregular solution of the Laplace equation).

where  $H_{KS} = H_{KS}(r)$  is the Kohn-Sham Hamiltonian in the real space. Then, one possible choice of the  $m$  unit-orbitals is

$$|j\rangle = |j\rangle + |j\rangle (\hat{H} - \hat{E}): \quad (9)$$

In this paper we use the shorthanded notations by Andersen et al. For instance, Eq. (9) should be read as follows:

$$|j_{RL}\rangle = |j_{RL}\rangle + \sum_{R^0L^0} |j_{R^0L^0}\rangle (H_{R^0R}^{L^0L} - E_{R^0L^0} E_L):$$

The first and second terms in the right-hand side of this equation are sometimes called, correspondingly, the "head" and the "tail" of MTO. The angular character of MTO at the central site  $R$  is specified by that of partial wave  $R_L$ . The matrix elements of  $H_{KS}$  in the MTOs basis (9) can be immediately derived by using the properties (4)–(8) of  $R_L$  and  $-R_L^0$ :

$$\langle j | H_{KS} | j \rangle = \hat{H} + (\hat{H} - \hat{E}) \hat{p} (\hat{H} - \hat{E});$$

where  $\hat{E}$  and  $\hat{p}$  are the diagonal matrices constructed from  $\langle f | E_L \rangle$  and  $\langle f | p_{RL} \rangle$ , and  $\langle j | H_{KS} | j \rangle$  is the shorthanded notation for the matrix  $\langle j_{RL} | H_{KS} | j_{R^0L^0} \rangle$ . The corresponding overlap matrix,  $\langle j_{RL} | j_{R^0L^0} \rangle$ , is

$$\langle j | j \rangle = \hat{1} + (\hat{H} - \hat{E}) \hat{p} (\hat{H} - \hat{E}):$$

Since the second term in the right-hand side of  $\langle j | j \rangle$  is typically small, the basis functions (9) are said to form a nearly orthogonal representation of the LMTO method, and  $\hat{H}$  is the LMTO Hamiltonian in the second order of  $(\hat{H} - \hat{E})$ . The basis (9) can be orthonormalized numerically, by applying the transformation

$$|j\rangle \rightarrow |j\rangle = |j\rangle |j\rangle^{1/2}:$$

The corresponding LMTO Hamiltonian,  $\hat{H} = \langle j | H_{KS} | j \rangle$ , which is formally valid in all orders of  $(\hat{H} - \hat{E})$ , is given by

$$\hat{H} = \langle j | j \rangle^{1/2} \langle j | H_{KS} | j \rangle |j\rangle^{1/2}:$$

This Hamiltonian will be used as the starting point in the next section, for the definition of transfer interactions between certain Wannier orbitals. We start with the formal description of the downfolding method. The construction of the Wannier basis functions, underlying this approach, will be considered in Sec. IV, where we will use again all

merits of the LMTO method and show that proper WF's can be constructed by retaining the "heads" of MTOs and attaching to them different "tails".

For periodic crystals, it is convenient to work in the reciprocal ( $k$ ) space. Therefore, if it is not specified otherwise, we assume that the LMTO Hamiltonian is already constructed in the reciprocal space, after the Fourier transformation of MTOs:

$$j_{kL} = \frac{1}{N} \sum_R e^{ikR} j_{RL};$$

where  $N$  is the number of sites.

For all considered compounds, results of our ASA-LMTO calculations are in a good agreement with the ones obtained using more accurate full-potential methods. In our definition of the crystal-field splitting we go beyond the conventional ASA and take into account nonsphericity of the electron-ion interactions (see Sec. V).

### III. DOWNFOLDING METHOD FOR THE KINETIC-ENERGY PART

Parameters of the kinetic energy are obtained using the downfolding method, starting from the electronic structure in LDA. In order to describe properly the electronic structure of the TM oxides in the valent part of the spectrum using the LMTO method, it is typically required several tens or even hundreds basis functions (including the ones associated with empty spheres, which are added in order to improve the atomic spheres approximation for loosely packed atomic structures). Several examples of such bases will be given in Secs. VIA-VID.

What we want to do next is to describe some part of this electronic structure by certain tight-binding (TB) Hamiltonian  $\hat{H}$ , which, contrary to  $\hat{H}$ , is formulated in the basis of a very limited number of orthogonal atomic-like orbitals. For example, in order to reproduce the  $t_{2g}$  bands located near the Fermi level, one would like to use only three  $t_{2g}$  orbitals centered at each TM site. These orbitals have a meaning of Wannier orbitals, which will be considered in Sec. IV.

We start with the identity by noting that any eigenstate of the LMTO Hamiltonian  $\hat{H}$  can be presented as the sum  $j_i = j_{ti} + j_{ri}$ , where  $j_{ti}$  is expanded over the LMTO basis function of the  $t_{2g}$ -type,  $f_{j_{ti}}$  (here, the character of the basis function is specified by its "head"), and  $j_{ri}$  is expanded over the rest of the basis functions  $f_{j_{ri}}$ . Then, the matrix equations for LMTO eigenstates can be rearranged identically as

$$(\hat{H}^{tt} - \epsilon) j_{ti} + \hat{H}^{tr} j_{ri} = 0; \quad (10)$$

$$\hat{H}^{rt} j_{ti} + (\hat{H}^{rr} - \epsilon) j_{ri} = 0; \quad (11)$$

By eliminating  $j_{ri}$  from Eq. (11) one obtains the effective  $\epsilon$ -dependent Hamiltonian in the basis of  $t_{2g}$ -states

$$\hat{H}_e^{tt}(\epsilon) = \hat{H}^{tt} - \hat{H}^{tr} (\hat{H}^{rr} - \epsilon)^{-1} \hat{H}^{rt}$$

and the "overlap" matrix

$$\hat{S}(\epsilon) = 1 + \hat{H}^{tr} (\hat{H}^{rr} - \epsilon)^{-1} \hat{H}^{rt};$$

satisfying the condition  $\sum_i \hat{S}^{-1} j_{ti} = 1$ . Then, the required TB Hamiltonian,  $\hat{H}$ , is obtained after the orthonormalization of the vectors  $j_{ti}$ :  $\tilde{j}_{ti} = \hat{S}^{1/2} j_{ti}$  and fixing the energy  $\epsilon$  in the center of gravity of the  $t_{2g}$  band ( $\epsilon_0$ ):

$$\hat{H} = \hat{S}^{-1/2} (\epsilon_0) \hat{H}_e^{tt}(\epsilon_0) \hat{S}^{1/2} (\epsilon_0); \quad (12)$$

Typically, the downfolding is performed in the reciprocal space, and the parameter  $\epsilon_0$  may also depend on  $k$ . The Hamiltonian  $\hat{H}_k$  can be Fourier transformed back to the real space:

$$\hat{H}_{RR^0} = \sum_k e^{ik(R-R^0)} \hat{H}_k;$$

The site-diagonal part of  $\hat{H}_{RR^0}$  shall describe the crystal-field (CF) splitting caused by the lattice distortion and associated with the transfer interactions between  $t$ - and  $r$ -orbitals, which are eliminated in the downfolding method, while the off-diagonal elements have a meaning of transfer interactions. The first application of this approach has been considered in Ref. 11. In Sec. VI we will illustrate abilities of this method for several types of  $t_{2g}$  compounds.

The crystal-field splitting may have another origin, which is related with nonsphericity of the electron-ion interactions.<sup>12</sup> This contribution will be considered in Sec. V.



## A . Spacial extension of Wannier functions

The choice of the WFs as well as their extension in the real space is not uniquely defined. For many practical applications one would like to have "maximally localized" orbitals,<sup>13</sup> although in the context of the WFs, the term "maximally localized" itself bears certain arbitrariness and is merely a mathematical construction, because depending on the considered physical property one can introduce different criteria of the "maximal localization".

Although we do not explicitly employ here any procedure which would pick up the "most localized" representation for the WFs, our method well suits this general strategy and the obtained WFs are expected to be well localized around the central TM sites.

There are several ways of controlling the spacial extension of the WFs in the LMTO method.

1. By using different envelop functions one can, in principle, change the spacial extension of MTOs (Fig. 2), which controls the decay of the original LMTO Hamiltonian in the real space. For example, instead of irregular solutions of Laplace equation, one can use Hankel functions of the complex argument. However, any choice should satisfy certain criteria of the completeness of the basis set. From this point of view, the use of the Hankel functions is not well justified as it typically deteriorates the accuracy of LMTO calculations. Therefore, in the present work we leave this problem as it is and fix the LMTO basis set.

2. Once the LMTO basis is fixed, the relative weight of the TM d-states and other atomic states which contribute to the  $t_{2g}$  band cannot be changed (see Fig. 1). For example, the contribution of the oxygen 2p-states cannot be replaced by  $\mu$ -n-tin orbitals centered at the TM sites and vice versa. The same proportion of atomic orbitals should be preserved in the WFs, constructed for this  $t_{2g}$  band. Then, the only parameter which can be controlled is how many WFs, centered at different sites of the lattice, contribute to the density of d-states at the given TM site. Then, the definition "localized orbital" mean that it is mainly centered around given TM site. Conversely, the "delocalized orbital" may have a long tail spreading over other TM sites. Then, it is easy to see that our procedure corresponds to the former choice. Indeed, in the first order of  $(\hat{h} - \hat{E}_t)$  and neglecting for a while the nonorthogonality to the rest of the electronic states, the norm of the WF can be obtained from Eq. (16) as  $\langle \tilde{W} | \tilde{W} \rangle_i = h_{tj}^{-1} h_{ti}$ , meaning that the WF is fully localized at the central TM site. Then, it holds  $\hat{h} = \hat{h}_i$ , which is valid in the second order of  $(\hat{h} - \hat{E}_t)$ .<sup>10</sup> Therefore, the leading correction to the above approximation, which defines the actual weight of the WF at the neighboring TM sites is controlled by the parameters of the kinetic energy  $\hat{h}$ , and is of the order of  $\hat{h}_i \hat{p}_i \hat{h}_i$ . As we will see below, the latter is small. The conclusion is rather generic and well anticipated for the strongly-correlated systems for which the kinetic-energy terms is generally small.

3. The angular character of the WF at the central TM site should be consistent with the one extracted from the local density of states in the region of  $t_{2g}$  bands (in the other words, the local density of states at the TM sites should be well represented by atomic orbitals  $f_{j \sim t, i, g}$  used in the downfolding method). Therefore, we choose  $f_{j \sim t, i, g}$  as the set of atomic orbitals which mainly contribute to the local density of states in the region of  $t_{2g}$  bands. For these purposes, at each TM site we calculate the density matrix in the basis of  $f_{j \sim d, i, g}$ :

$$\hat{N} = \sum_{i \in t_{2g}} h_{dj}^{-1} h_{ij} f_{j \sim d, i, g} \quad (19)$$

and sum up the contributions of all  $t_{2g}$  bands (here,  $i$  is an joint index, which incorporates the band index and the coordinates of the  $k$ -point in the first Brillouin zone). Then, we diagonalize  $\hat{N}$ , and assign three most populated orbitals, obtained after the diagonalization to  $f_{j \sim t, i, g}$ .

## V . CRYSTAL-FIELD SPLITTING CAUSED BY NONSPHERICITY OF ELECTRON-ION INTERACTIONS

The contribution of Coulomb interactions to the crystal-field splitting is a tricky issue. Despite an apparent simplicity of the problem, one should clearly distinguish different contribution and not to include them twice, in the kinetic and Coulomb parts of the model Hamiltonian (3). The use of full-potential techniques does not automatically guarantee the right answer. However, the atomic-spheres-approximation, which typically supplements the LMTO method, will also require additional corrections for the crystal-field splitting. In this section we would like to make two comments on this problem.

1. The nonsphericity of on-site Coulomb interactions is already included in the second part of the model Hamiltonian (3). The problem will be discussed in details in Sec. VII. Therefore, in order to avoid the double counting, the corresponding contribution to the kinetic-energy part should be subtracted. From this point of view the use of the spherically averaged KS potential in ASA is well justified.

The same is true for the intersite Coulomb interactions, if they are explicitly included to the model Hamiltonian (3).

2. All remaining interactions should generally contribute to the crystal-field splitting. In ASA, the proper correction at the site  $R$  can be found by considering the matrix elements of the Coulomb potential produced by all other atomic spheres (or ions) at the site  $R$ ,

$$\hat{h}_{RR} = \sum_{R' \neq R} W_{R'} \int \frac{Z_{R'} e^2}{|\mathbf{R} + \mathbf{r} - \mathbf{R}'|} W_{R'} d\mathbf{r};$$

where  $W_{R'} = W_{R'}(\mathbf{r})$  is the WF centered at the site  $R'$ , and  $Z_{R'}$  is the total charge associated with the sphere  $R'$ : namely, the nuclear charge minus the electronic charge encircled by the atomic sphere. The nonspherical part of this integral can be easily calculated in the real space by using the multipole expansion for  $|\mathbf{R} + \mathbf{r} - \mathbf{R}'|^{-1}$ .

In all forthcoming discussions, unless it is specified otherwise, the matrix elements of the crystal-field splitting will incorporate the correction  $\hat{h}_{RR}$  associated with nonsphericity of the electron-ion interactions.

## V I. A P P L I C A T I O N S T O T R A N S I T I O N - M E T A L O X I D E S

### A . C u b i c P e r o v s k i t e s : S r V O <sub>3</sub>

SrVO<sub>3</sub> is a rare example of perovskite compounds, which crystallizes in the ideal cubic structure. It attracted a considerable attention in the connection with the bandwidth control of the metal-insulator transition.<sup>5</sup>

For the cubic compounds, the separation of the LMTO basis functions into  $f_{j \sim t_2g}$  and  $f_{j \sim e_g}$  used in the downfolding method is rather straightforward: three  $t_{2g}$  orbitals centered at each V site form the subspace of  $f_{j \sim t_2g}$  orbitals, and the rest of the basis functions are associated with  $f_{j \sim e_g}$ .

Parameters of LMTO calculations for SrVO<sub>3</sub> are given in Table I. The corresponding electronic structure is shown

TABLE I: Atomic positions (in units of cubic lattice parameter  $a = 3.842 \text{ \AA}$ ), atomic radii (in  $\text{\AA}$ ) and basis functions included in LMTO calculations for cubic SrVO<sub>3</sub>.

type of atom	position	atomic radius	LMTO basis	number of atoms
Sr	(0.5;0.5;0.5)	1.919	5s5p4d4f	1
V	(0;0;0)	1.470	4s4p3d	1
O	(0.5;0;0)	1.032	2s2p	3

in Fig. 3. The downfolding procedure is nearly perfect and well reproduces the behavior of three  $t_{2g}$  bands. As

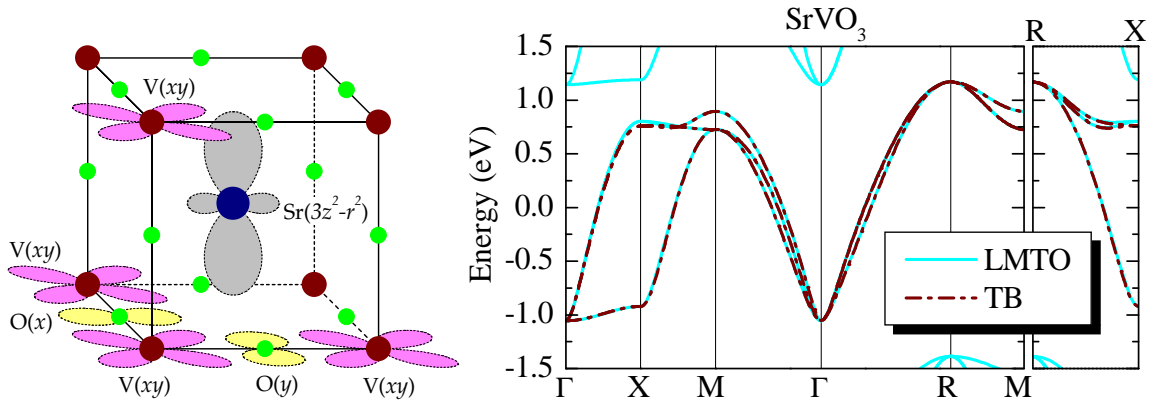


FIG. 3: Left panel: Crystal structure of cubic perovskites and atomic wavefunctions mediating transfer interactions between V ( $t_{2g}$ ) orbitals. The standard V(xy)-O(y)-V(xy) and V(xy)-O(x)-V(xy) interactions operate in the x- and y-directions, respectively. The V(xy)-Sr( $3z^2-r^2$ )-V(xy) interaction operates in the "forbidden" z-direction. Right panel: LDA energy bands for SrVO<sub>3</sub> obtained in LMTO calculations and after the tight-binding (TB) parametrization using the downfolding method. Notations of the high-symmetry points of the Brillouin zone are taken from Ref. 14.

expected for cubic perovskite compounds,<sup>15</sup> the transfer interactions between different  $t_{2g}$  orbitals are small. The



dispersion of  $t_{2g}$  bands is well described in terms of three interaction parameters  $t_1$ ,  $t_1^0$ , and  $t_2$ :

$$t_{xy}(\mathbf{k}) = 2t_1(\cos a k_x + \cos a k_y) + 2t_1^0 \cos a k_z + 4t_2 \cos a k_x \cos a k_y$$

( $a$  being the cubic lattice parameter; similar expressions for the  $yz$  and  $zx$  bands are obtained by cyclic permutations of the indices  $x$ ,  $y$ , and  $z$ ). The parameters  $t_1$ ,  $t_1^0$ , and  $t_2$ , obtained after the Fourier transformation, are listed in Table II. As expected, the nearest-neighbor (NN) dd -interaction  $t_1$  mediated by the oxygen 2p-states is the strongest.

TABLE II: Parameters of transfer interactions for  $\text{SrVO}_3$  (in eV).

$t_1$	$t_1^0$	$t_2$
0.209	0.023	0.084

For the  $xy$ -orbitals, it operates in the  $x$  and  $y$  directions. However, there is also an appreciable dd -interaction  $t_1^0$  operating in the "forbidden" direction (for example, the direction  $z$  in the case of  $xy$  orbitals). These interactions are mediated by the  $\text{Sr}(4d)$  states and strongly depend on the proximity of the latter to the Fermi level. Therefore, it is not quite right to say that the transfer interactions between  $t_{2g}$  orbitals are strictly two-dimensional in the cubic lattice.<sup>16</sup> Since the  $\text{La}(5d)$  states are located even lower in energy than the  $\text{Sr}(4d)$  ones, the interaction  $t_1^0$  is expected to be even stronger in  $\text{LaTiO}_3$ . However, in the case of  $\text{LaTiO}_3$  we have an additional complication associated with the orthorhombic distortion. As we will see below, it changes the conventional form of transfer interactions expected for the simplified cubic perovskite structure dramatically.

The corresponding WF is shown in Fig. 4. In this case, the  $t$ -part of the WF was constructed from the  $3d$ - $t_{2g}$

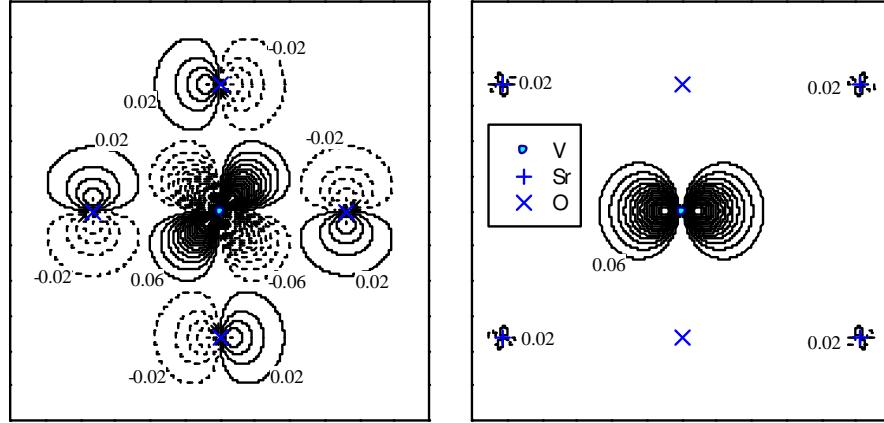


FIG. 4: Contour plot of the  $xy$ -Wannier orbital of  $\text{SrVO}_3$ , in the (001) (left) and  $(\bar{1}10)$  (right) planes. The solid and dashed line correspond to the positive and negative values of the Wannier function. Atomic positions are shown by symbols. A round each site, the Wannier function increases/decreases with the step 0.04 from the values indicated on the graph.

partial waves inside V spheres. The partial waves of the  $\text{Sr}(4d5s)$ ,  $\text{V}(3d-e_g)$ , and  $\text{O}(2p)$  types were included into the  $r$ -part, in order to enforce the orthogonality of the WF to the bands of the aforementioned type.

Since the  $t_{2g}$  band is an antibonding combination of the atomic  $\text{V}(3d-t_{2g})$  and  $\text{O}(2p)$  orbitals, the WF has nodes located between V and O sites. Fig. 5 illustrates the spacial extension of the WF. It shows the electronic charge accumulated around the central V site after adding every new sphere of the neighboring atomic sites. Since the WF is normalized, the total charge should be equal to one. In the case of  $\text{SrVO}_3$ , 77% of this charge belongs to the central V site, 16% is distributed over four neighboring oxygen sites, about 5% belongs to the next eight Sr sites, and 1% to the eight oxygen sites located in the fourth coordination sphere. Other contributions are small.

It is also instructive to calculate the expectation value of the square of the position operator,  $\langle r^2 \rangle = \langle \mathbf{r}^2 \rangle = \int \mathbf{r}^2 |\Psi|^2 d\mathbf{r}$ , which characterizes the spread of the WF in the method of Marzari and Vanderbilt.<sup>13</sup> They proposed to define the "maximally localized" Wannier orbitals as the ones which minimize  $\langle r^2 \rangle$ . Using the WF shown in Fig. 4, we obtain  $\langle r^2 \rangle = 2.37 \text{ \AA}^2$ . Unfortunately, at present all applications of the method by Marzari and Vanderbilt to the TM oxides are limited by MNO.<sup>17</sup> Therefore, we can make only indirect comparison between two different compounds. The values of  $\langle r^2 \rangle$  reported in Ref. 17 for individual WFs centered at the Mn and O sites were of the order of  $0.6\text{--}0.8 \text{ \AA}^2$ , that is

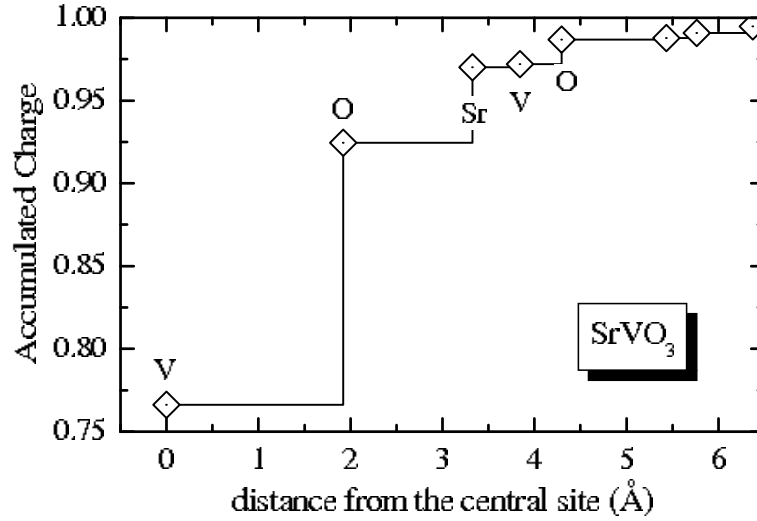


FIG. 5: Spatial extension of  $t_{2g}$ -Wannier function in  $\text{SrVO}_3$ : the electronic charge accumulated around the central V site after adding every new sphere of neighboring atomic sites.

considerably smaller than  $2.37 \text{ \AA}^2$  obtained in our work for  $\text{SrVO}_3$ . However, such a difference is not surprising.

1. Our scheme of constructing the WFs is not based on the minimization of  $\langle r^2 \rangle$ . Therefore, our values of  $\langle r^2 \rangle$  should be generally larger.

2. More importantly, the spatial extension of the WFs depends on the dimensionality of the Hilbert space, which is used in the construction of the Hubbard model. For example, we will show in Sec. V D that by treating explicitly the  $e_g$  states in  $\text{V}_2\text{O}_3$  one can easily find more compact representation for the Wannier orbitals. This characteristic can be further improved by including the O ( $2p$ ) states explicitly into the Wannier basis,<sup>18</sup> like in Ref. 17 for  $\text{MnO}$ . However, there is a very high price to pay for this extra localization. This is the dimensionality of the Hilbert space, which becomes crucial in the many-body methods for the numerical solution of the model Hamiltonian (3).

Thus, we believe that our WFs constructed for isolated  $t_{2g}$  band are indeed well localized.

For cubic perovskites, there are several ways of extracting parameters of transfer interactions from the first-principles electronic structure calculations. For example, one can simply fit the LDA band structure in terms of a small number of Slater-Koster interactions.<sup>15</sup> However, the situation becomes increasingly complicated in materials with the lower crystal symmetry, like the orthorhombically distorted perovskite oxides, corundum, or pyrochlore compounds. First, the number of possible Slater-Koster interactions increases dramatically. Second, the form of these interactions becomes very complicated and differs substantially from the cubic perovskite compounds (one example is the mixing of  $t_{2g}$  and  $e_g$  orbitals by the orthorhombic distortion, which does not occur in cubic perovskites). Therefore, it seems that for complex compounds the only way to proceed is to use the downfolding method. In the next sections we will consider several examples along this line.

## B. Orthorhombically Distorted Perovskites: $\text{YTiO}_3$

$\text{YTiO}_3$  is a ferromagnetic insulator. The recent interest to this compound has been spurred by the behavior of orbital polarization, which is closely related with the origin of the ferromagnetic ground state.  $\text{YTiO}_3$  is typically considered in combination with  $\text{LaTiO}_3$ , which is an antiferromagnetic insulator. The magnetic behavior of these two, formally isoelectronic materials, is not fully understood.<sup>11</sup>

Contrary to  $\text{SrVO}_3$ , both  $\text{YTiO}_3$  and  $\text{LaTiO}_3$  crystallize in the strongly distorted orthorhombic structure (shown in Fig. 6 for  $\text{YTiO}_3$ , the space group No. 62 in the International Tables; the Schönflies notation is  $D_{2h}^{16}$ ). In this section we will illustrate abilities of the downfolding method for distorted perovskite compounds, using  $\text{YTiO}_3$  as an example. Parameters of LMTO calculations for  $\text{YTiO}_3$  are given in Table III.

A new problem we have to address here is how to separate the basis functions of the LMTO method onto the  $f_{j_{\text{t}}}$  and  $f_{j_{\text{r}}}$  orbitals. Note that although the  $t_{2g}$  band is well separated from the rest of the electronic structure also in the case of  $\text{YTiO}_3$ , the atomic  $t_{2g}$  and  $e_g$  orbitals are strongly mixed by the crystal field effects and the transfer interactions in the distorted perovskite structure. Therefore, the conventional separation into atomic  $t_{2g}$  orbitals and

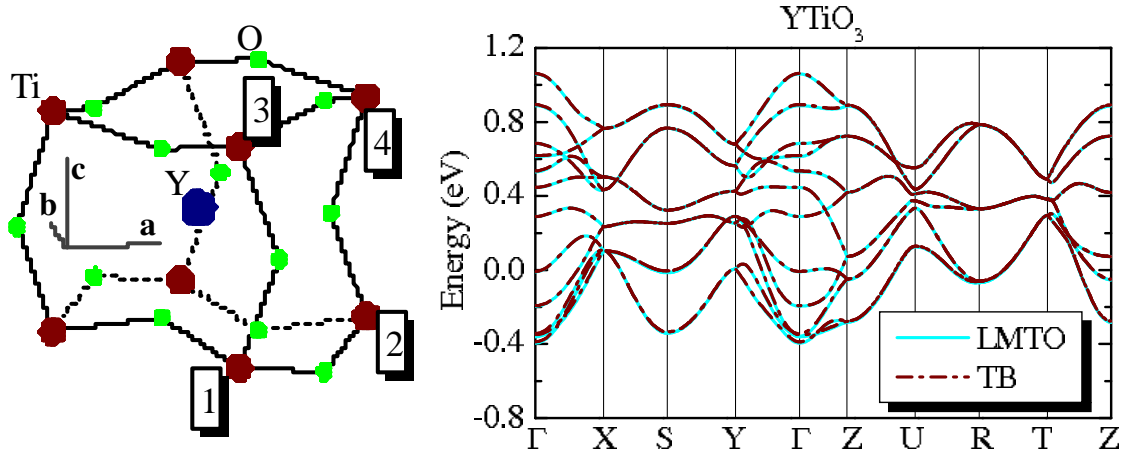


FIG. 6: Left panel: Fragment of crystal structure of  $\text{YTiO}_3$  (a "distorted cube"). The inset shows the directions of orthorhombic axes. Right panel: LDA energy bands for  $\text{YTiO}_3$  obtained in LMTO calculations and after tight-binding (TB) parametrization using the downfolding method. Notations of the high-symmetry points of the Brillouin zone are taken from Ref. 14.

TABLE III: Atomic positions (in units of orthorhombic lattice parameters  $a = 5.316$ ,  $b = 5.679$ , and  $c = 7.611 \text{ \AA}$ ), atomic radii (in Å) and basis functions included in LMTO calculations for orthorhombically distorted  $\text{YTiO}_3$ . The symbol Em' stands for the empty spheres.

type of atom	position	atomic radius	LMTO basis	number of atoms
Y	(0.521; 0.073; 0.250)	1.758	5s5p4d4f	4
Ti	(0; 0; 0)	1.507	4s4p3d	4
O	(0.379; 0.458; 0.250)	1.052	2s2p	4
O	(0.309; 0.191; 0.558)	1.043	2s2p	8
Em	(0.192; 0.268; 0.116)	0.595	1s	8
Em	(0.438; 0.329; 0.750)	0.757	1s2p	4
Em	(0.149; 0.368; 0.027)	0.556	1s	8
Em	(0.106; 0.208; 0.199)	0.479	1s	8

the rest of the basis functions does not apply here, and in order to generate  $f_{j\sim i}$  we use eigenvectors of the density matrix (see Sec. IV A).

For the site 1, shown in Fig. 6, these three " $t_{2g}$  orbitals" have the following form (in the basis of  $\hat{x}y_i$ ,  $\hat{y}z_i$ ,  $\hat{z}^2_i$ ,  $\hat{x}x_i$ , and  $\hat{x}^2 - \hat{y}^2_i$  orbitals, in the orthorhombic coordinate frame):

$$\begin{aligned}
 \tilde{j}_{1i} &= (0.13; 0.60; 0.24; 0.34; 0.67); \\
 \tilde{j}_{2i} &= (0.17; 0.50; 0.35; 0.77; 0.11); \\
 \tilde{j}_{3i} &= (0.43; 0.54; 0.29; 0.22; 0.62);
 \end{aligned} \tag{20}$$

At the sites 2, 3, and 4 similar orbitals can be generated from the ones at the site 1 using the symmetry properties of the  $D_{2h}^{16}$  group and applying the 180° rotations around the orthorhombic axes  $a$ ,  $c$ , and  $b$ , respectively. These orbitals define the local basis (or the local coordinate frame) around each Ti site.

Then, the rest of the basis functions  $f_{r\sim g}$  can be eliminated using the downfolding method. The corresponding electronic structure for the  $t_{2g}$  bands is shown in Fig. 6, which reveals an excellent agreement between results of LMTO calculations and their tight-binding parametrization using the down-folding method.

Parameters obtained after the transformation to the real space are listed in Table IV, in the local coordinate frame. We note a substantial crystal-field splitting associated with the orthorhombic distortion. After the diagonalization of the site-diagonal part of the TB Hamiltonian  $\hat{H}_i$ , we obtain the following ("one-down, two-up") splitting of  $t_{2g}$  levels: 0.076, 0.032, and 0.046 eV. Some implications of the crystal-field splitting to the orbital polarization and the magnetic ground state of  $\text{YTiO}_3$  and  $\text{LaTiO}_3$  have been discussed in Refs. 11 and 12.<sup>19</sup> The form of transfer interactions becomes extremely complicated, and differs dramatically from many naive expectations based on the

TABLE IV : Parameters of the kinetic energy for  $\text{YTiO}_3$  (in eV), in the local coordinate frame. The atomic positions are shown in Fig. 6. The basis functions at the site 1 are given by Eqs. (20). The basis functions at the sites 2 and 3 are obtained by the 180° rotations of the site 1 around the orthorhombic axes  $a$  and  $c$ , respectively. The matrix  $\hat{h}_{11}$  describes the crystal-field splitting at the site 1 (nonsphericity of electron-ion interactions has been added in  $\hat{h}_{11}$ ). The matrices  $\hat{h}_{12}$  and  $\hat{h}_{13}$  stand for the transfer integrals in the bonds 1-2 and 1-3, respectively.

$i-j$	$\hat{h}_{ij}$		
1-1	0.060	0.039	0.014
	0.039	0.028	0.001
	0.014	0.001	0.032
1-2	0.080	0.036	0.072
	0.162	0.013	0.073
	0.063	0.031	0.038
1-3	0.000	0.080	0.055
	0.080	0.082	0.007
	0.055	0.007	0.073

analogy with the cubic perovskites. Generally, the transfer interactions are three-dimensional and operate between different  $t_{2g}$  orbitals.

The WFs are shown in Fig. 7, and their spacial extension in the real space is illustrated in Fig. 8. In these calculations, the WFs have been orthogonalized to the O (2p), Ti(3d- $e_g$ ), and Y (4d) bands. The orbitals appear

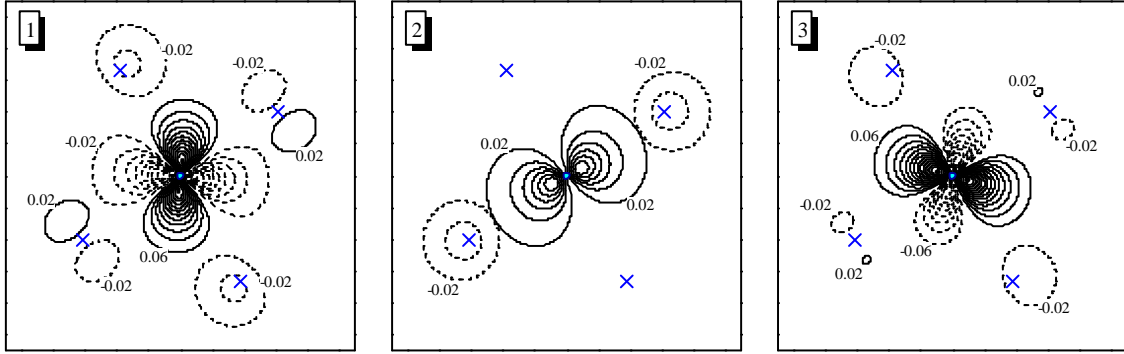


FIG. 7: Contour plot of three  $t_{2g}$ -Wannier orbitals in the (001) plane of  $\text{YTiO}_3$ . The orbitals are centered at the site 1 shown in Fig. 6. Projections of the vanadium and oxygen sites onto the plane are shown by circles and crosses, respectively. Other notations are the same as in Fig. 4.

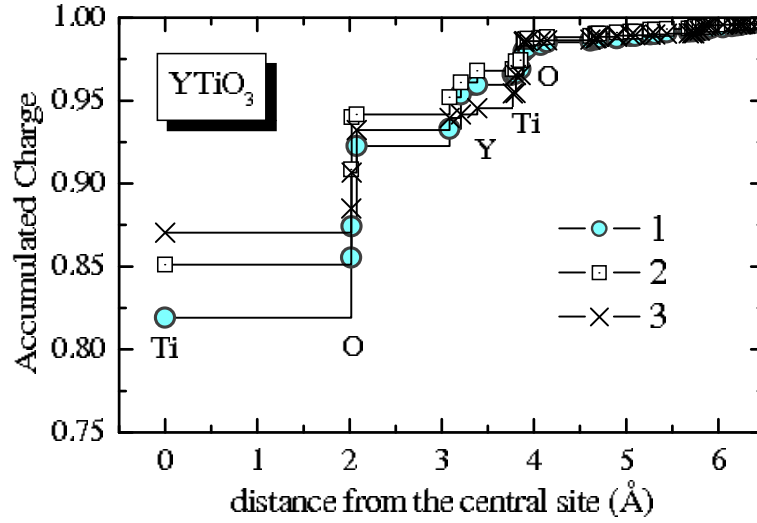
to be more localized than in  $\text{SrVO}_3$ : 82-87% of the total charge belongs to the central Ti site, and only 6 to 10% is distributed over neighboring oxygen sites. This is because of the large orthorhombic distortion, which suppresses all interatomic interactions mediated by the oxygen states. Another reason is the larger energy distance between O (2p) and  $t_{2g}$  bands in  $\text{YTiO}_3$  (3.2 eV against 0.3 eV in  $\text{SrVO}_3$  (see Fig. 1)), which explains a smaller weight of the atomic oxygen states in the  $t_{2g}$  band and the WFs of  $\text{YTiO}_3$ .

Another interesting feature is that the degree of localization is pretty different for three orbitals. For example, we obtain  $\langle r^2 \rangle = 2.28, 1.90$ , and  $2.05 \text{ \AA}^2$ , correspondingly for  $W_1, W_2$ , and  $W_3$  shown in Fig. 7. One can paraphrase it in a different way: the degree of hybridization can be different for different  $t_{2g}$  orbitals, unless they are related with each other by symmetry operations.

### C. Pyrochlores: $\text{Y}_2\text{M}_2\text{O}_7$

The pyrochlore compounds exhibit a variety of interesting properties. Many of them are not fully understood.

$\text{Y}_2\text{M}_2\text{O}_7$  is a canonical example of geometrically frustrated systems. In this compound, the magnetic atoms form the networks of corner-sharing tetrahedra. Then, the antiferromagnetic coupling between NN M spins leads to the

FIG. 8: Spatial extension of  $t_{2g}$ -Wannier functions in  $YTiO_3$ .

frustration. The origin of this antiferromagnetic coupling can be understood on the basis of semi-empirical Hartree-Fock calculations.<sup>20</sup> A remaining question, which is not fully understood, is the origin of the spin-glass state realized in  $Y_2M_2O_7$  below 20 K.<sup>21</sup> For comparison,  $Nd_2M_2O_7$  is a ferromagnet, revealing a large anomalous Hall effect.<sup>20,22</sup>

Another interesting group is superconducting pyrochlores with the chemical formula  $AO_2O_6$  ( $A = K, Rb$ , and  $Cs$ ).<sup>23</sup>

In this section we will derive parameters of the kinetic energy for the  $t_{2g}$  band of  $Y_2M_2O_7$ . Very similar strategy can be applied for other pyrochlores. Parameters of LMTO calculations for  $Y_2M_2O_7$  are listed in Table V.

TABLE V: Atomic positions (in units of cubic lattice parameter  $a = 10.21$  Å), atomic radii (in Å) and basis functions included in LMTO calculations for pyrochlore  $Y_2M_2O_7$ .

type of atom	position	atomic radius	LMTO basis	number of atoms
Y	(0.5;0.5;0.5)	1.746	5s5p4d	4
Mo	(0;0;0)	1.587	5s5p4d	4
O	(0.375;0.375;0.375)	1.032	2s2p	2
O	(0.338;0.125;0.125)	1.032	2s2p	12
Em	(0.125;0.125;0.125)	0.952	1s2p3d	2
Em	(0.25;0;0)	1.044	1s2p3d	8

In the pyrochlore lattice, each Mo site is located in the trigonal environment (Fig. 9). Therefore, the atomic Mo( $t_{2g}$ ) levels will be split into one-dimensional  $a_{1g}$  and two-dimensional  $e_g$  representations. The latter states can mix with the Mo( $e_g$ ) states, which belong to the same representation. Therefore, the basis functions  $f_{j\tau i}$  can be constructed in the same manner as for  $YTiO_3$ , by diagonalizing the site-diagonal part of the density matrix for the  $t_{2g}$  bands. For the site 1 shown in Fig. 9, this yields the following atomic orbitals (in the basis of  $\tilde{y}z$ ,  $\tilde{z}x$ ,  $\tilde{x}y$ , and  $\tilde{y}^2 - \tilde{z}^2$  orbitals):

$$\begin{aligned}
 f_{1i} &= (0.58; 0.58; 0; 0.58; 0); \\
 f_{2i} &= (0.06; 0.18; 0.29; 0.13; 0.93); \\
 f_{3i} &= (0.18; 0.04; 0.93; 0.14; 0.29);
 \end{aligned} \tag{21}$$

In these notations, the first orbital corresponds to the  $a_{1g}$  representation, and two others to the  $e_g$  representation. Similar orbitals at the sites 2, 3, and 4 can be generated from the ones at the site 1 using the symmetry operations of the  $O_h$  group (No. 227 in the International Tables): namely, the 180° rotations around the cubic axes  $x$ ,  $y$ , and  $z$ , respectively. The rest of the basis functions form the subspace  $f_{j\tau i}$ .

The electronic structure obtained after the elimination of the  $f_{j\tau i}$  orbitals is shown in Fig. 9. Again, we note an excellent agreement with the results of the original LMTO calculations. The parameters of the kinetic energy in the

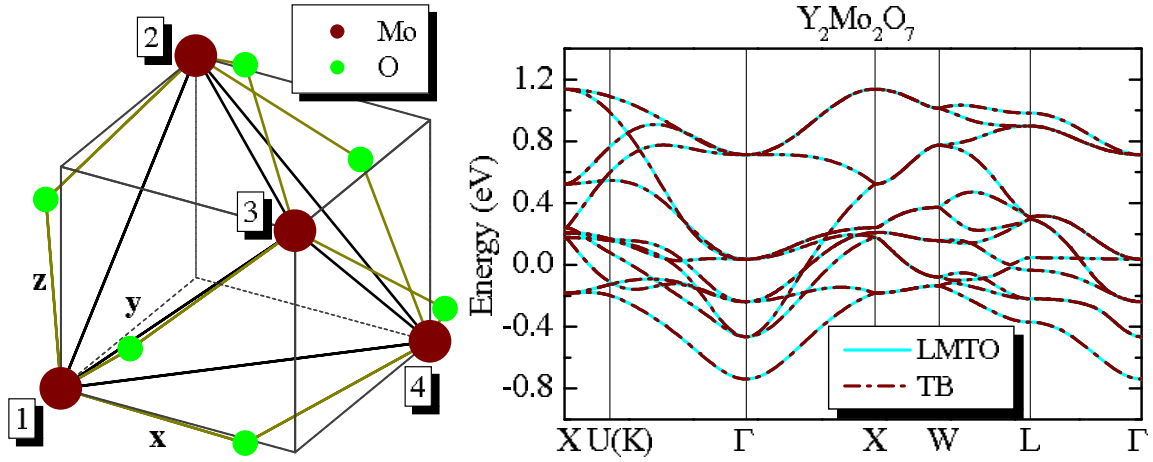


FIG. 9: Left panel shows the fragment of crystal structure of  $Y_2Mo_2O_7$ : a single  $MoO_4$  tetrahedron surrounded by the oxygen sites. In  $Y_2Mo_2O_7$ , the Y and Mo ions from two sublattices of corner-sharing tetrahedra. The sublattices interpenetrate in a way, in which each Mo is located in the center of Y hexagon (not shown here). Right panel: LDA energy bands for  $Y_2Mo_2O_7$  obtained in LMTO calculations and after tight-binding (TB) parametrization using the downfolding method. Notations of the high-symmetry points of the Brillouin zone are taken from Ref. 14.

real space are listed in Table VI. We note an appreciable ( $\sim 0.25$  eV) crystal-field splitting between the  $a_{1g}$  and  $e_g$

TABLE VI: Parameters of the kinetic energy for  $Y_2Mo_2O_7$  (in eV), in the local coordinate frame. The atomic positions are shown in Fig. 9. The basis orbitals at the site 1 are given by Eqs. (21). The basis orbitals at the sites 2, 3, and 4 are obtained by the 180° rotations of the site 1 around the cubic axes  $x$ ,  $y$ , and  $z$ , respectively. The matrix  $\hat{h}_{11}$  describes the crystal-field splitting at the site 1 (nonsphericity of electron-ion interactions has been added in  $\hat{h}_{11}$ ). The matrix  $\hat{h}_{14}$  stands for transfer integrals between atoms 1 and 4.

$i-j$	$\hat{h}_{ij}$		
1-1	0.177	0.000	0.000
	0.000	0.088	0.000
	0.000	0.000	0.088
1-4	0.064	0.001	0.002
	0.001	0.186	0.070
	0.002	0.070	0.022

orbitals.<sup>20</sup> The NN transfer interactions in the bonds other than 1-4 can be obtained using the symmetry operations of the  $O_h^7$  group. The transfer interactions beyond the nearest neighbors are considerably smaller.

The corresponding WFs are shown in Fig. 10, and their spacial extension is depicted in Fig. 11. The WFs have been orthogonalized to the neighboring Y ( $4d-e_g$ ) and O ( $2p$ ) bands. Since the  $4d$ -wavefunctions are typically more extended in comparison with the  $3d$  ones, the WFs are less localized. In the case of  $Y_2Mo_2O_7$ , 75-80% of the total charge is located at the central site, and about 20% is distributed over neighboring oxygen sites. The degree of localization also depends on the symmetry of WFs. So, the  $a_{1g}$  orbital is well localized within the  $MoO_4$  cluster, whereas the  $e_g$  orbitals have a noticeable weight ( $\sim 2.5\%$  of the total charge) at the Y and Mo sites belonging to the next coordination sphere.

#### D. Corundum-type $V_2O_3$

$V_2O_3$  is regarded as the canonical Mott-Hubbard system, where the Coulomb interaction between conduction electrons leads to a breakdown of the conventional one-electron band theory.<sup>24</sup> It was and continues to be the subject of vast research activity, which has been summarized in many review articles (for instance, Ref. 5).

$V_2O_3$  crystallizes in the corundum structure with two formula units per rhombohedral cell (the space group is  $D_{3d}^6$ , No. 167 in the International Tables). The local environment of the V sites is trigonal (Fig. 12), in which the  $t_{2g}$  levels

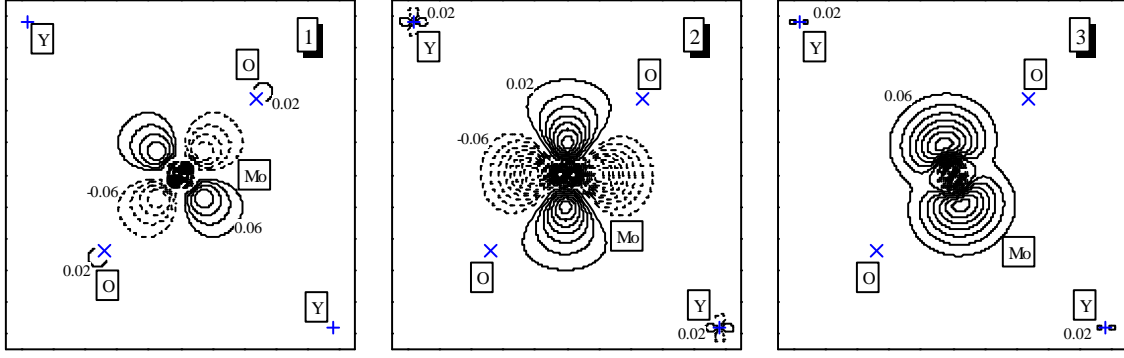


FIG. 10: Contour plot of three  $t_{2g}$ -W annier orbitals in the (001) plane of  $Y_2Mo_2O_7$ . The orbitals correspond to the site 1 in Fig. 9. The orbital 1 corresponds to the  $a_{1g}$  representation, the orbitals 2 and 3 correspond to the  $e_g$  representation. Other notations are the same as in Fig. 4.

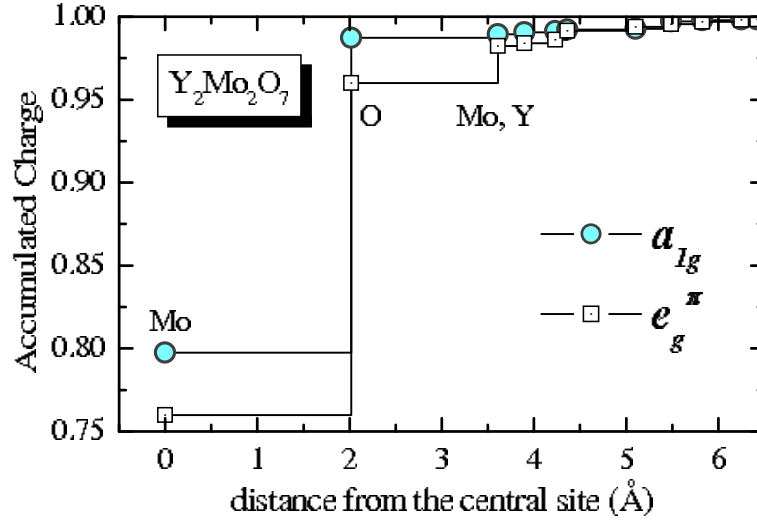


FIG. 11: Spatial extension of  $t_{2g}$ -W annier functions in  $Y_2Mo_2O_7$ .

are split into one-dimensional  $a_{1g}$  and two-dimensional  $e_g$  representations.

Parameters of LMTO calculations for  $V_2O_3$  are given in Table V II.

TABLE V II: Atomic positions (in units of rhombohedral lattice parameters  $a=2.859$  and  $c=4.667$  Å), atomic radii (in Å) and basis functions included in LMTO calculations for  $V_2O_3$ .

type of atom	position	atomic radius	LMTO basis	number of atoms
V	(0;0;0.5)	1.317	4s4p3d	4
O	(0.5;0.326;0.25)	1.009	2s2p3d	6
Em	(0;0;0)	1.223	1s2p3d	2
Em	(0.5;0.267;0.25)	0.921	1s2p	6

In the present work, our main interest in  $V_2O_3$  will be purely academic. As we can see in Fig. 1,  $V_2O_3$  has two well separated bands, which are mainly formed by the V (3d) states. One is the  $t_{2g}$  band, which in LDA is crossed by the Fermi level. Another one is the  $e_g$  band, which is located around 3 eV, and composed mainly of the  $e_g$  states. The latter can mix with the  $e_g$  ones. Therefore, for  $V_2O_3$  (and related corundum-type oxides) one can introduce two different models.

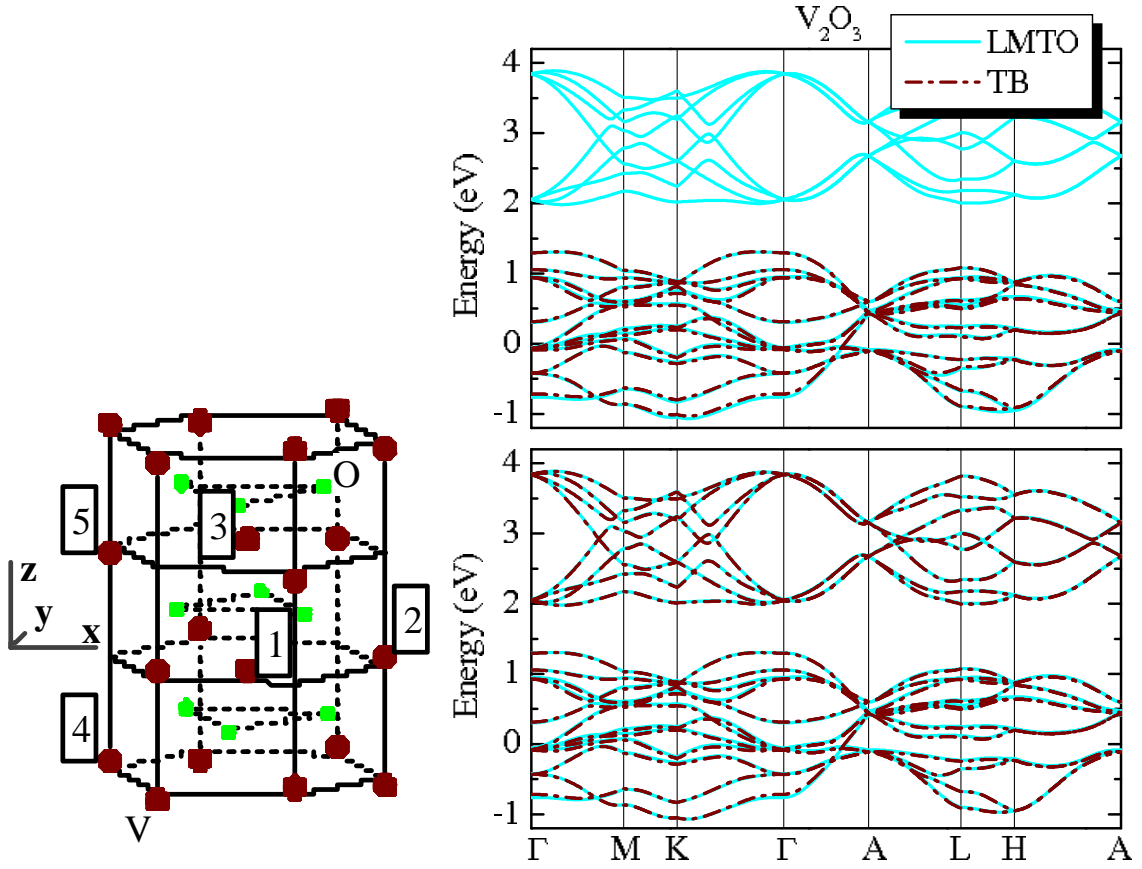


FIG. 12: Left panel: Crystal structure of  $V_2O_3$  with the notation of atomic sites. The sites 3 and 4 are equivalent and can be transformed to each other by primitive translations (both atomic positions are required in order to specify the form of transfer integrals in Table V III). Right panel: LDA energy bands for  $V_2O_3$  obtained in LMTO calculations and after tight-binding (TB) parametrization using the downfolding method for the three-orbital (top) and ve-orbital (bottom) models. Notations of the high-symmetry points of the Brillouin zone are taken from Ref. 14.

The first one is more general and explicitly treats all V (3d) bands. In the following we will call it as the “ve-orbital” model, according to the number of basis orbitals  $f_{\text{ve}}^{\text{orb}} = 12$  per one V site. The oxygen degrees of freedom will be eliminated using the downfolding method. The corresponding TB Hamiltonian will be denoted as  $\hat{h}^{(5)}$ .

The second one is the minimal model, which can be derived from the previous one by eliminating the  $e_g$  states. We will call it the “three-orbital” model. The corresponding TB Hamiltonian will be denoted as  $\hat{h}^{(3)}$ .

The basic difference between these two models is that the first one treats the  $e_g$  states explicitly, while in the second case the effect of these states is included implicitly, through the renormalization of interaction parameters between  $a_{1g}$  and  $e_g$  orbitals.

For both models, the local orbitals at each V site were obtained from the diagonalization of the density matrix, which sums up the contributions over twelve  $t_{2g}$  bands. For the three-orbital model, such choice of the basis functions is very important, as it controls the accuracy of the downfolding method. For the ve-orbital model, one can use any unitary transformation of the ve 3d orbitals. Obviously, the final result will not depend on this transformation. However, for a better comparison between two models, we use the same basis in both cases. In principle, the  $e_g$  and  $e_g$  states will be mixed in the density matrix, as they belong to the same representation. However, we will continue to call the lower- and upper-lying  $e_g$  states as  $e_g$  and  $e_g$ , despite the fact that each of them may have an admixture of another type.

Then, the basis orbitals at the sites 1 and 2 (see Fig. 12) have the following form (in the basis of atomic  $\hat{p}_x, \hat{p}_y, \hat{p}_z, \hat{p}_x^2, \hat{p}_y^2, \hat{p}_z^2$  orbitals):

$$\begin{aligned} \hat{p}_1 &= (0.77; 0.29; 0; 0.48; 0.30); \\ \hat{p}_2 &= (0.30; 0.48; 0; 0.29; 0.77); \end{aligned}$$



$$\begin{aligned}
j_{\sim 3}i &= (0 \ ; \ 0 \ ; \ 1 \ ; \ 0 \ ; \ 0 \ ); \\
j_{\sim 4}i &= (0\cdot49; \ 0\cdot51; \ 0 \ ; \ 0\cdot65; \ 0\cdot27); \\
j_{\sim 5}i &= (0\cdot27; \ 0\cdot65; \ 0 \ ; \ 0\cdot51; \ 0\cdot49);
\end{aligned} \tag{22}$$

In these notations,  $j_{\sim 1}i$  and  $j_{\sim 2}i$  are the  $e_g$  orbitals,  $j_{\sim 3}i$  is the  $a_{1g}$  orbital, and  $j_{\sim 4}i$  and  $j_{\sim 5}i$  are the  $e_g$  orbitals. The basis orbitals at the sites 3, 4, and 5 are generated by the mirror-reflection  $y \rightarrow y$  in Eq. (22). In the three-orbital model, first three orbitals constitute the subspace  $fj_{\sim t}ig$ , while two remaining orbitals are included in  $fj_{\sim r}ig$ . In the  $v$ -orbital model, all  $v$ -orbitals are included in  $fj_{\sim t}ig$ .

The electronic structure obtained after the downfolding is shown in Fig. 12. The three-orbital model well reproduces the behavior of twelve  $t_{2g}$  bands, while the  $v$ -orbital model allows to reproduce both  $t_{2g}$  and  $e_g$  bands.

The corresponding parameters in the real space are given in Table V III. In the  $v$ -orbital model, one can see a noticeable hybridization between  $t_{2g}$  and  $e_g$  states. Therefore, the elimination of the  $e_g$  states in the three-orbital model should lead to an additional renormalization of the parameters of the crystal-field splitting and the transfer interactions. Generally, the matrix elements of the kinetic-energy part in the subspace of  $t_{2g}$  orbitals are not the same for two considered models.

TABLE V III: Parameters of the kinetic energy (in eV) in the local coordinate frame for three- and  $v$ -orbital models of  $V_2O_3$  (denoted as  $\hat{h}_{ij}^{(3)}$  and  $\hat{h}_{ij}^{(5)}$ , respectively). The atomic positions are shown in Fig. 12. The basis functions at the sites 1 and 2 are given by Eqs. (22). The basis functions at the sites 3, 4, and 5 are obtained by the reflection  $y \rightarrow y$  of the site 1. The order of orbitals is  $e_g$ ,  $a_{1g}$ , and  $e_g$ . The  $e_g$  orbitals are eliminated in the three-orbital model.

$i-j$	$\hat{h}_{ij}^{(3)}$			$\hat{h}_{ij}^{(5)}$				
1-1	0.053	0.000	0.000	0.141	0.000	0.000	0.008	0.056
	0.000	0.053	0.000	0.000	0.141	0.000	0.056	0.008
	0.000	0.000	0.107	0.000	0.000	0.190	0.000	0.000
				0.008	0.056	0.000	2.326	0.000
				0.056	0.008	0.000	0.000	2.326
1-2	0.024	0.089	0.103	0.009	0.080	0.104	0.026	0.043
	0.089	0.150	0.207	0.080	0.103	0.202	0.085	0.102
	0.103	0.207	0.025	0.104	0.202	0.032	0.114	0.068
				0.026	0.085	0.114	0.067	0.030
				0.043	0.102	0.068	0.030	0.042
1-3	0.037	0.027	0.000	0.032	0.054	0.000	0.064	0.163
	0.027	0.037	0.000	0.054	0.032	0.000	0.163	0.064
	0.000	0.000	0.342	0.000	0.000	0.331	0.000	0.000
				0.064	0.163	0.000	0.014	0.065
				0.163	0.064	0.000	0.065	0.014
1-4	0.089	0.024	0.102	0.112	0.013	0.113	0.053	0.002
	0.024	0.018	0.024	0.013	0.000	0.048	0.356	0.029
	0.102	0.024	0.125	0.113	0.048	0.124	0.092	0.004
				0.053	0.356	0.092	0.213	0.031
				0.002	0.029	0.004	0.031	0.000
1-5	0.053	0.053	0.019	0.046	0.060	0.027	0.076	0.175
	0.004	0.039	0.034	0.002	0.050	0.046	0.069	0.151
	0.047	0.113	0.054	0.071	0.105	0.050	0.020	0.032
				0.124	0.017	0.055	0.039	0.078
				0.259	0.041	0.161	0.133	0.234

As an example, we show in Table IX the crystal-field splitting between  $e_g$  and  $a_{1g}$  levels for the series of corundum-type oxides, obtained after the diagonalization of the matrices  $\hat{h}_{11}^{(3)}$  and  $\hat{h}_{11}^{(5)}$ . The splitting turns out to be very different in two different models. Since many properties of TM oxides are controlled by this crystal-field splitting,<sup>25</sup> such a model-dependence may be viewed as somewhat unphysical. However, the crystal-field splitting cannot be considered independently from other model parameters, such as the Coulomb and transfer interactions, which should be defined on the same footing and for the same type of model. For the Coulomb interactions, it is important to follow the

concept of WFs, which we will consider in the next section.

TABLE IX: Parameters of crystal-field splitting between  $e_g$  and  $a_{1g}$  levels obtained for the series of corundum-type oxides in the three- ( $^{(3)}_{CF}$ ) and ve- ( $^{(5)}_{CF}$ ) orbital models. The positive value of  $^{(3)}_{CF}$  means that the  $a_{1g}$  level lies higher than  $e_g$ . The nonsphericity of electron-ion interactions has been included (the values in parenthesis show the crystal-field splitting originating from the transfer interactions alone).

compound	$^{(3)}_{CF}$ (eV)	$^{(5)}_{CF}$ (eV)
$Ti_2O_3$	0.070 (0.254)	-0.033 (0.159)
$V_2O_3$	0.160 (0.233)	0.051 (0.128)
$Cr_2O_3$	0.140 (0.216)	0.051 (0.129)

We also note an appreciable contribution coming from nonsphericity of the electron-ion interactions. This contribution, which is ignored in conventional ASA, acts against the crystal-field splitting originating from the transfer interactions and tends to stabilize the  $a_{1g}$  level. This may revise certain conclusions obtained in the framework of ASA-LMTO method.<sup>25</sup>

Corresponding WFs are shown in Fig. 13, and their spacial extension  $\{$  in Fig. 14. All functions have been

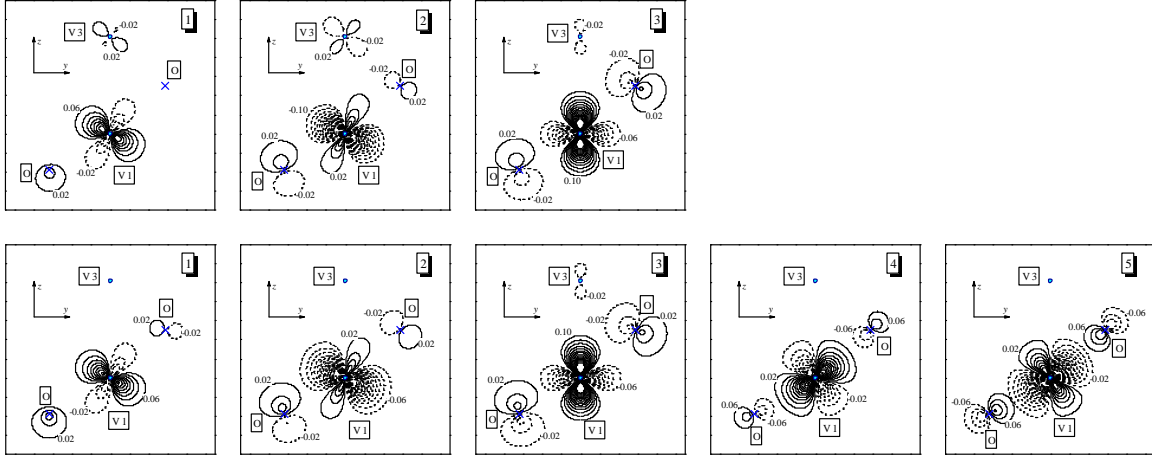


FIG. 13: Contour plot Wannier orbitals in the (100) plane of  $V_2O_3$ , obtained in the three-orbital (top) and ve-orbital (bottom) models. Projections of the vanadium and oxygen sites onto the plane are shown by circles and crosses, respectively. The numbering of V atoms (V1" and V3") is the same as in Fig. 12. First two orbitals (1 and 2) are of the  $e_g$  type, third orbital (3) is of the  $a_{1g}$  type, and last two orbitals (4 and 5) are of the  $e_g$  type. Other notations are the same as in Fig. 7.

orthogonalized to the O (2p) band. In the three-orbital model, the WFs have been additionally orthogonalized to the V ( $e_g$ ) band. Similar to  $Y_2M_2O_7$ , the spacial extension of the WFs strongly depends on their symmetry. Generally, the  $a_{1g}$  and  $e_g$  orbitals are more localized, while the  $e_g$  orbitals have a considerable weight (more than 20% of the total charge) at the neighboring oxygen sites. Furthermore, the spacial extension of the WFs depends on the model for which they are constructed. Generally, the ve-orbital model allows to construct more compact WFs rather than the three-orbital one. For example, in the three-orbital model we have  $\langle r^2 \rangle = 1.75$  and  $2.38 \text{ \AA}^2$ , correspondingly for the  $a_{1g}$  and  $e_g$  orbitals. For comparison, the ve-orbital yields  $\langle r^2 \rangle = 1.04, 1.04$ , and  $1.41 \text{ \AA}^2$  for the  $a_{1g}$ ,  $e_g$ , and  $e_g$  orbitals, respectively.

This is not surprising.

1. The transfer interactions in the three-orbital model are longer-ranged, as they contain additional contributions mediated by the  $e_g$  orbitals.

2. For the three-orbital model, the WFs should be additionally orthogonalized to the V ( $e_g$ ) band. At the central site, this condition can be easily satisfied by choosing proper atomic  $t_{2g}$  and  $e_g$  orbitals, which diagonalize the density matrix. However, the WF has a tail spreading to the neighboring sites, which should be additionally orthogonalized to the V ( $e_g$ ) band by including partial waves of the  $e_g$  type into the r-part of the WF.

Thus, there is certain compromise with the choice of the suitable model for compounds like  $V_2O_3$ , where smaller dimensionality of the Hilbert space in the three-orbital model is counterbalanced by necessity to deal with more extended WFs.

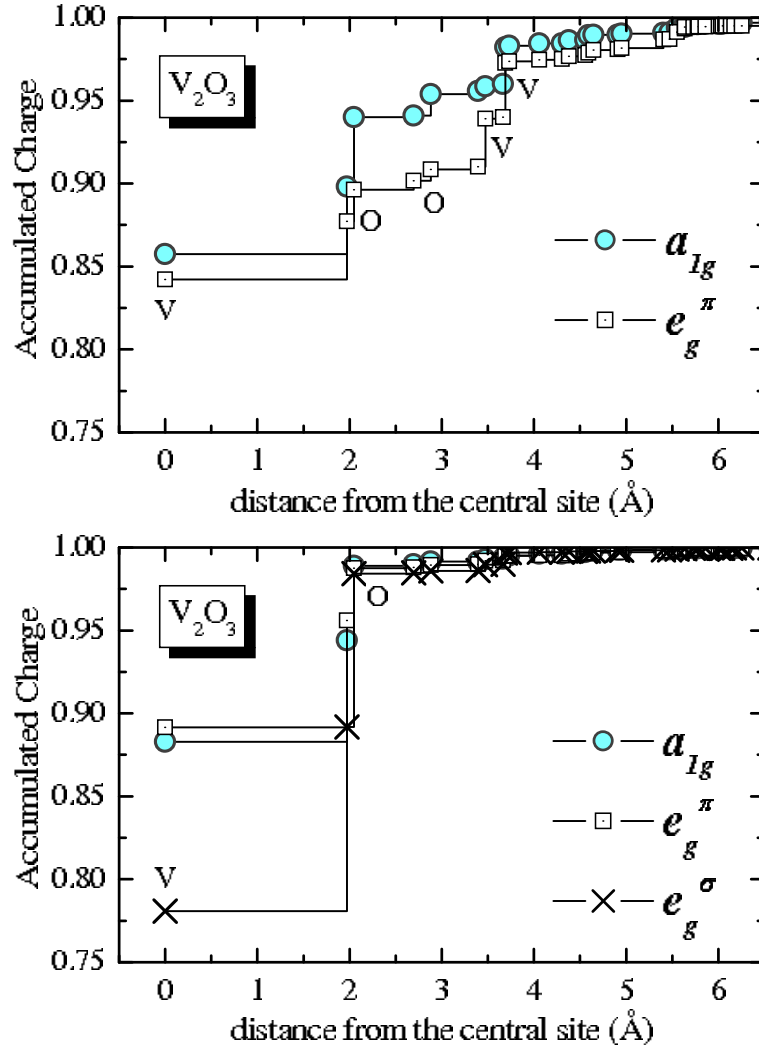


FIG. 14: Spatial extension of Wannier functions in the three- (top) and five- (bottom) orbital models for  $V_2O_3$ .

## VII. THE EFFECTIVE COULOMB INTERACTION

The calculation of effective Coulomb interactions for the first principles is an extremely complicated problem because they are subjected to different mechanisms of screening which should be taken into consideration in the process of these calculations. So far, the solution of this problem has not been fully accomplished by any of the research groups, despite a vast activity in this direction.<sup>26,27,28,29,30,31,32,33,34,35,36,37,38,39,40</sup> It would be probably fair to say from the very beginning that we were not able to solve this problem either, without additional approximations, which will be considered in Sec. V IIA. However, we hope to present certain systematics on different points of view, which can be found in the literature. We will also summarize several open questions and unresolved problems.

It is convenient to start with the basic definition of the effective Coulomb interaction  $U$ , as it was discussed in many details by Herring.<sup>41</sup> According to this definition, (the spherically averaged part of)  $U$  is nothing but the energy cost for the reaction  $2(d^n) \rightarrow d^{n+1} + d^{n-1}$ , i.e. for moving a  $d$ -electron between two atoms, located at  $R$  and  $R^0$ , and initially populated by  $n_R = n_{R^0} = n$  electrons:

$$U = E[n_R + 1; n_{R^0} - 1] - E[n_R; n_{R^0}]. \quad (23)$$

This  $U$  may depend on  $R$  and  $R^0$ , and using several combinations of  $R$  and  $R^0$  one can extract the values of both on-site and intersite interactions. A typical example for  $SrVO_3$  will be considered in Sec. V IIB. However, here we drop these atomic indices and consider more general aspects of calculations of the effective Coulomb interactions.

It is implied that the electron is transferred between two Wannier orbitals, and  $n_R$  and  $n_{R^0}$  are the populations

of these Wannier orbitals. A special precaution should be taken in order to avoid the double counting of the kinetic energy term. Indeed, since the kinetic-energy term is included explicitly into the Hubbard model (3), it should not contribute to the total energy difference (23). This point was emphasized by Gunnarsson and co-workers, in the series of publications.<sup>30,31,32</sup> They proposed to derive  $U$  from constraint-LDA (c-LDA) calculations,<sup>26</sup> and suppress all matrix elements of hybridization involving the atomic d-states. Such a procedure can be easily implemented in the LMTO method. For the 3d-compounds, this method typically yields  $U \approx 5-12$  eV<sup>3,35</sup>, which is too large (if correct, results of this approach would imply that all nature surrounding us would be "strongly correlated"). Therefore, although the basic strategy is correct, there is an important piece of physics, which is missing in the method of Gunnarsson et al.

Similar strategy can be pursued in our WF method. Our basic idea is to switch off the kinetic-energy term during the construction of the WFs, and to use these functions in calculations of the effective interaction  $U$ . Therefore, instead of regular WFs  $\hat{w}(\mathbf{r})$ , which after applying to the KS Hamiltonian generate the matrix  $\hat{H}_{KS} \hat{w}(\mathbf{r}) = \hat{\epsilon}$ , we introduce the set of auxiliary Wannier functions  $\hat{w}(\mathbf{r})$ , satisfying the condition  $\hat{H}_{KS} \hat{w}(\mathbf{r}) = \hat{\epsilon}$ . In the ground-state configuration ( $n_R = n_{R^0} - n$ ),  $\hat{\epsilon}$  is a constant, which can be dropped.<sup>42</sup> In the excited state ( $n_R \neq n_{R^0}$ ),  $\hat{\epsilon}$  is a diagonal matrix with respect to the site indices,  $\hat{\epsilon} = \epsilon_{RR^0}$ , where each matrix element  $\epsilon_{RR^0}$  may depend on occupation numbers  $f_{n_R}$ . Since such auxiliary WFs do not interact with each other through the kinetic-energy term, they can be used as the basis functions for the effective Coulomb interaction  $U$ .

The auxiliary WFs can be easily constructed using the method proposed in Sec. IV after the substitution  $\hat{h} = \hat{\epsilon}$  in all equations. Meanwhile, the orthogonality condition to other LDA bands is strictly observed by including proper solutions of KS equations inside atomic spheres and their energy derivatives into the  $r$ -part of auxiliary WFs. This allows to retain the hybridization between TM d- and oxygen p-states, which is an important feature of TM oxides. As we will see below, the change of this hybridization, induced by the reaction  $2(d^n) \rightarrow d^{n+1} + d^{n-1}$ , represents a very important channel of screening, which substantially reduces  $U$  and explains many details of its behavior in solids. This channel of screening has been overlooked by Gunnarsson et al.

A similar idea, although formulated in the very different way, has been recently proposed by Aryasetiawan et al.<sup>39</sup> They proposed to extract the parameter  $U$  from the GW method,<sup>43,44</sup> and suppressed all contributions to the GW polarization function associated with the transitions between Hubbard (in our case  $t_{2g}$ ) bands, in order to avoid the double counting of these effects in the process of solution of the Hubbard model. Clearly, since the polarization function in the GW method will vanish without the kinetic-energy term, this procedure appears to be similar to the setting  $\hat{h} = \hat{\epsilon}$  for the WFs, which are used as the basis functions for the effective Coulomb interaction  $U$ .

A characteristic example of the auxiliary WFs is shown in Fig. 15 for  $\text{SrVO}_3$ . We note only a minor difference

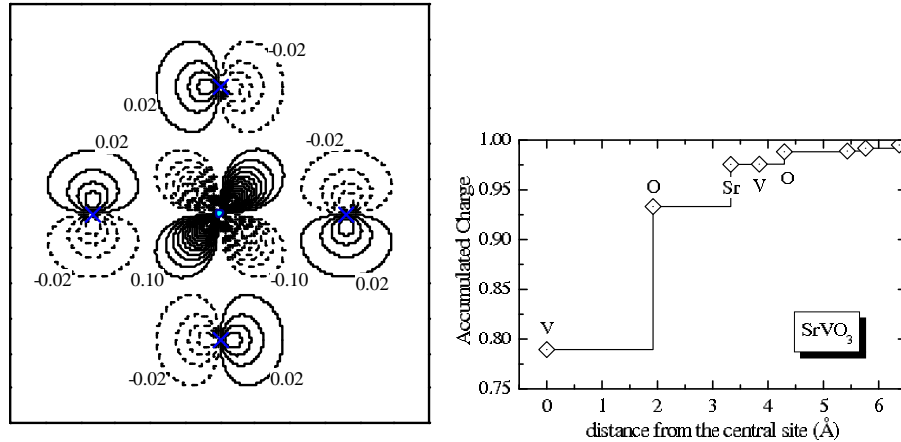


FIG. 15: An example of auxiliary Wannier function  $\hat{w}(\mathbf{r})$  for  $\text{SrVO}_3$  for which all parameters of the kinetic energy are set to be zero. Left panel shows the contour plot of the  $xy$ -orbital in the (001) plane. Right panel shows the spatial extension of this orbital. Other notations are the same as in Figs. 4 and 5.

between auxiliary WFs and the regular ones shown in Fig. 4, meaning that the main details of the WFs for the  $t_{2g}$  bands are predetermined by orthogonality condition to other bands. For example, in the case of auxiliary WFs, 79% of the total charge are accumulated at the central V site (instead of 77% for the regular WFs). The values of  $\langle r^2 \rangle$  obtained for the auxiliary and regular WFs are 2.27 and 2.37 Å, respectively. Thus, the auxiliary WFs appear to be more localized. However, the difference is small. The result is well anticipated for strongly correlated systems, for which the kinetic-energy term  $\hat{h}$  is expected to be small.

Since the KS Hamiltonian is diagonal in the basis of auxiliary WFs, the latter can be regarded as eigenstates of this Hamiltonian corresponding to certain boundary condition. The corresponding set of KS eigenvalues will be denoted as  $\epsilon_R$ . Then, the occupation numbers  $f_{R\sigma}$  become well defined and one can use the standard properties of the density-functional theory. Namely, by using Janak's theorem for the KS eigenvalues

$$\epsilon_R = \frac{\partial E}{\partial n_R}$$

and Slater's transition-state arguments, Eq. (23) can be further rearranged as

$$U = \epsilon_R \left[ n_R + \frac{1}{2}; n_{R^0} - \frac{1}{2} \right] - \epsilon_R \left[ n_R - \frac{1}{2}; n_{R^0} + \frac{1}{2} \right];$$

The final expression for the parameter  $U$  is obtained by considering the deviations  $\pm 1/2$  from  $n_R$  and  $n_{R^0}$  as a weak perturbation and employing the Taylor expansion. Then, in the first order of  $\pm 1/2$  one obtains:

$$U = \frac{\epsilon_R}{n_R}; \quad (24)$$

where the energy derivative is calculated under the following condition:

$$n_R + n_{R^0} = \text{const}; \quad (25)$$

which guarantees the conservation of the total number of particles. Strictly speaking, the definition (24) corresponds to the infinitesimal change of the occupation numbers  $2(d^n - d^{n+1} + d^{n-1})$ , which is different from original Herring's definition (23). However, for practical purposes, these definitions can be regarded as equivalent as they yield very similar values for the parameter  $U$ .<sup>33</sup>

Then, it is convenient to use the Hellmann-Feynman theorem, which allows to relate  $U$  with the change of the Hartree potential (the change of the exchange-correlation potential in LDA is typically small and can be neglected):<sup>33</sup>

$$U = \hbar \omega \left[ \frac{\partial V_H}{\partial n_R} \right];$$

Taking into account that  $V_H(r) = e^2 \int d\mathbf{r}^0 \rho(\mathbf{r}^0) / |\mathbf{r} - \mathbf{r}^0|$ , and using Eq. (2) for the electron density, the above expression can be rearranged as

$$U = e^2 \int d\mathbf{r} \int d\mathbf{r}^0 \frac{\rho(\mathbf{r}^0) \rho(\mathbf{r})}{|\mathbf{r} - \mathbf{r}^0| n_R};$$

where

$$\frac{\rho(\mathbf{r})}{n_R} = \sum_i \frac{n_i}{n_R} \rho_i(\mathbf{r}) + n_i \frac{1}{n_R} \rho_i(\mathbf{r}) \quad ; \quad (26)$$

The last expression points out at the existence of two additive channels of screening.

(i) The first one comes from the change of occupation numbers. Due to the constraint (25) imposed on the occupation numbers, this channel involves two Wannier orbitals, centered at different TM sites, and describes the screening of on-site Coulomb interactions by intersite interactions. Other states can be affected by this term only through the change of wavefunctions in the process of iterative solution of the KS equations. We also would like to note that this channel of screening is absent in the GW methods, which may lead to an error for metallic compounds.<sup>40</sup>

(ii) The second channel describes the relaxation of the wavefunctions. It affects both the auxiliary WFs and the electronic states belonging to the rest of the spectrum.

## A. Approximations and Simplifications

The usual way in calculating the parameter  $U$  is the c-LDA approach, that is to solve iteratively Eqs. (1) and (2) for a fixed set of occupation numbers  $f_{R\sigma}$ , which does not necessarily follow the Fermi-Dirac distribution for the ground state.<sup>26,27,28,29,30,31,32,33</sup> In practical calculations, these occupation numbers are controlled by an external potential  $V_{\text{ext}}(\mathbf{r})$ , playing a role of Lagrange multipliers in the constrained density functional theory. In spite of many limitations for the strongly correlated systems, LDA is formulated as the ground-state theory. Therefore, there is a

general belief that it should provide a good estimate for the total energy difference given by Eq. (23) and all other expressions which can be derived from Eq. (23) using usual arguments of DFT.

From the practical point of view, the basic difficulty of combining c-LDA with the WF method is the necessity to deal with relaxation of these WFs. This means that the auxiliary WFs should be recalculated on each iteration, for every new value of the electron density and the KS potential. Taking into account an arbitrariness with the choice of the WFs, this procedure cannot be easily implemented in the standard c-LDA calculations. Instead, we will employ a hybrid method, which starts with c-LDA and then takes into account the effects of relaxation of the WF in an analytical form, using the well-known expressions for the screened Coulomb interaction in the random-phase approximation (RPA).<sup>37,38,39,43,44</sup>

In c-LDA calculations, the change of the occupation numbers  $f_{n\mathbf{g}}$  is associated with some change of the total potential  $V = V_{\text{ext}} + V_{\text{H}} + V_{\text{XC}}$ . Then, the change of the electron density in Eq. (26) can be identically expressed in terms of the polarization function as

$$\rho(\mathbf{r}) = \int d\mathbf{r}' P(\mathbf{r}; \mathbf{r}') V(\mathbf{r}'). \quad (27)$$

Using Eq. (26), one can identify three main contributions to the polarization function associated with the following processes (correspondingly  $P^{\text{I}}$ ,  $P^{\text{II}}$ , and  $P^{\text{III}}$ ):

- I. the change of the occupation numbers of the auxiliary WFs;
- II. the relaxation of the auxiliary WFs;
- III. the relaxation of the rest of the electronic states.

Then, each  $W$  can be expressed in terms of the basis functions (or partial waves)  $f_{\mathbf{g}}$  and  $f_{-\mathbf{g}}$ , using Eq. (15). Therefore, the change of  $W$  includes the relaxation of these basis functions as well as the change of hybridization of the TM  $t_{2g}$  states with (mainly) the oxygen states. The latter is given by the change of coefficients  $f_{\mathbf{r}\mathbf{g}}$  in the right-hand side of Eq. (15). The corresponding contributions to the polarization function are denoted as  $P^{\text{IIB}}$  and  $P^{\text{IIH}}$ , which stand for the change of basis functions and hybridization, respectively. The same arguments are applied to relaxation of the rest of the electronic states. The corresponding polarization function can be divided accordingly in  $P^{\text{IIIB}}$  and  $P^{\text{IIIH}}$ . We also introduce combined notations:  $P^{\text{B}} = P^{\text{IIB}} + P^{\text{IIIB}}$  and  $P^{\text{H}} = P^{\text{IIH}} + P^{\text{IIIH}}$ .

We would like to point out here that, conceptually, the RPA approach for treating the relaxation effects is similar to c-LDA. The main difference is that RPA is based on an analytical expression for the change of the wavefunctions, formulated in terms of the perturbation theory expansion, while c-LDA treats the same effects numerically.<sup>40</sup> Therefore, we use a hybrid c-LDA+RPA scheme, which was originally considered in Ref. 40. It consists of two steps.

(i) First, we take into account the screening associated with  $P^{\text{I}}$ , and  $P^{\text{B}}$  in the framework of conventional c-LDA method, and neglect all kinds of hybridization effects involving the TM d-orbitals. An example of such a model electronic structure is shown in Fig. 16. This part is totally equivalent to the method of Gunnarsson and co-workers.<sup>30,31,32</sup> It allows to calculate the Coulomb repulsion  $u$  and the intra-atomic exchange (Hund's rule) coupling  $j = 2^2 E = m^2$  in the atomic limit ( $m$  being the spin magnetization). By using these  $u$  and  $j$  one can construct the full  $5 \times 5 \times 5 \times 5$  matrix  $\hat{u}$  of Coulomb interactions between atomic d electrons, as it is typically done in the LDA+U method.<sup>7,45</sup> This matrix will be used as the starting point in RPA calculations.

c-LDA is supplemented with additional approximations, such as the atomic-spheres approximation. It also disregards some hybridization effects. However, in Sec. V IIC we will see that at least for the static Coulomb interaction, the RPA results are close to the strong-coupling regime. In such a situation, the precise value of the parameter  $u$ , which is used as the starting point for these calculations, appears to be less important, and it is sufficient to have an "order of magnitude" estimate, which can be obtained from c-LDA. (ii) We turn on the hybridization, and evaluate the screening associated with the last portion of the polarization function,  $P^{\text{H}}$ , in RPA:

$$\hat{U} = \frac{1}{1 - \hat{P}^{\text{H}} \hat{u}} \hat{u}; \quad (28)$$

where  $\hat{P}^{\text{H}}$  is the  $5 \times 5 \times 5 \times 5$  matrix  $\hat{P}^{\text{H}}(\mathbf{k}, \mathbf{k})$ , which will be specified below.

Since total  $P$  is an additive function of  $P^{\text{I}}$ ,  $P^{\text{B}}$ , and  $P^{\text{H}}$ , this procedure can be justified within RPA, where each new contribution to the polarization function ( $P^{\text{H}}$ ) can be included consequently by starting with the Coulomb interaction  $\hat{u}$ , which already incorporates the effects of other terms ( $P^{\text{I}}$  and  $P^{\text{B}}$ ).<sup>39</sup>

The physical meaning of processes associated with the change of the hybridization and their role in the screening of local Coulomb interactions is illustrated schematically in Fig. 17.

Since the creation and the annihilation of an electron in RPA are treated as two independent processes, the screening of Coulomb interactions will be generally different from that associated with the true reaction  $2(d^n) \rightarrow d^{n+1} + d^{n-1}$ .

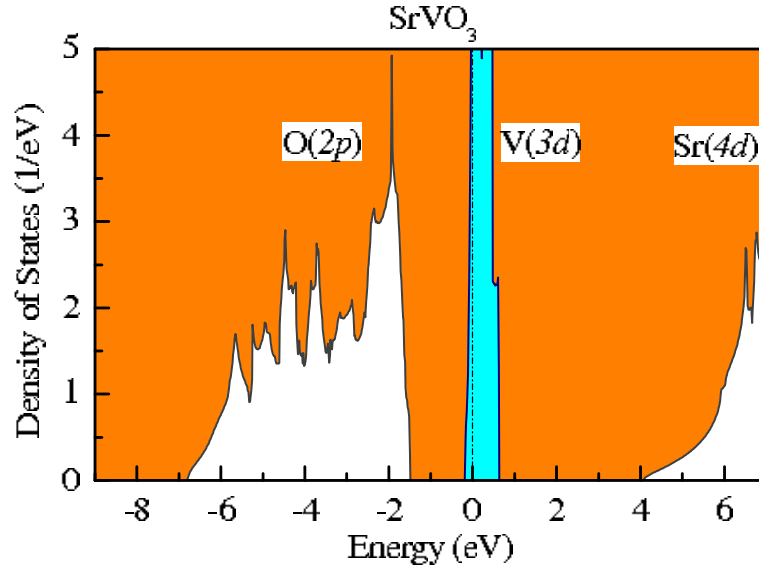


FIG. 16: An example of model electronic structure for  $\text{SrVO}_3$ , which is used in constraint-LDA calculations. The electronic structure corresponds to the canonical bands approximation.<sup>10</sup> The Fermi level is at zero energy.

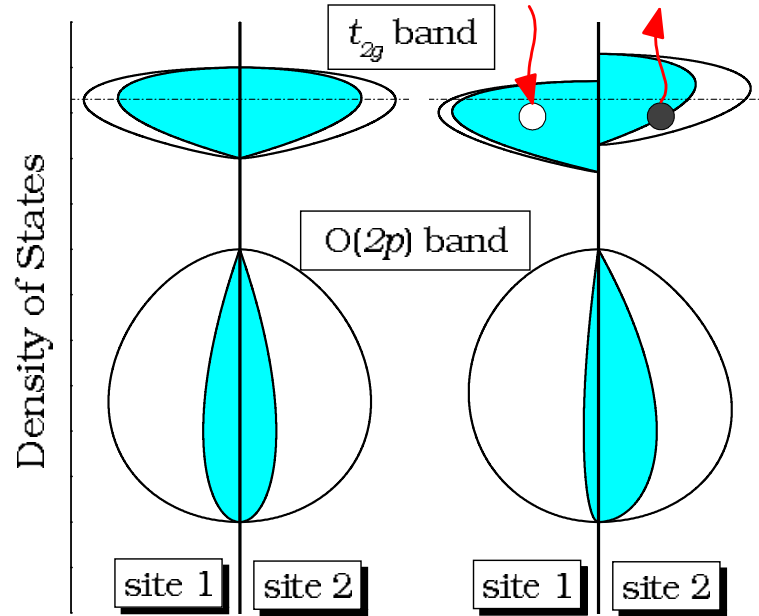


FIG. 17: A schematic view on the change of the p-d hybridization in the O (2p) and  $t_{2g}$  bands of the TM oxides associated with the repopulation of the Wannier orbitals at the neighboring transition-metal sites:  $2d^n \rightarrow d^{n+1} + d^{n+1}$ . Left panel corresponds to the ground-state configuration ( $2d^n$ ). In the right panel, the removal (addition) of an electron from (to) the Wannier orbital in the  $t_{2g}$  part of the spectrum is simulated by the shift of these orbitals relative to the Fermi level (shown by dot-dashed line). Around each transition-metal site, it changes the Coulomb potential, which controls the distribution of the d-states as well as the degree of their hybridization between TM (d) and O (2p) states. Generally, the removal of an electron from (or the addition of an electron to) the Wannier orbital is partially compensated by the change of the amount of d-states, which is admixed into the O (2p) band. This transfer of the spectral weight works as a very efficient channel of screening of local Coulomb interactions in the transition-metal oxides.

To some extent, the true screening can be simulated by imposing certain constraints on the form of RPA polarization function  $P^H$ . Namely, one can expect certain cancellation of contributions coming from Wannier orbitals centered at

different TM sites at the intermediate (i.e. oxygen) sites (see Fig. 18). Therefore, we believe that it is more physical

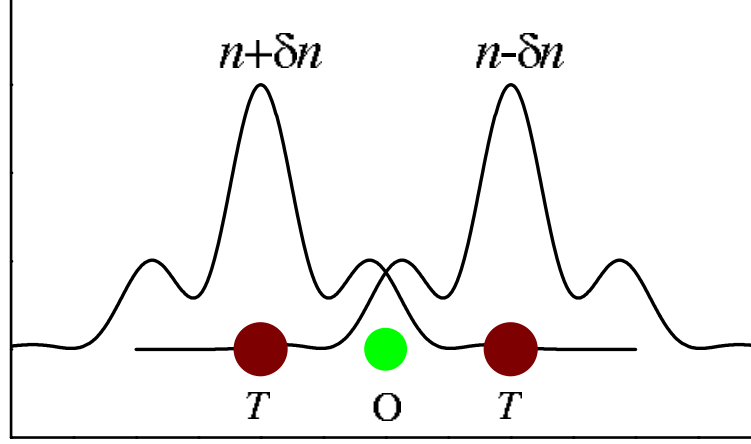


FIG. 18: A cartoon picture showing two Wannier orbitals centered at neighboring transition-metal sites (T) and having tails spreading to the intermediate oxygen (O) site. The charge disproportionation associated with the reaction  $2(d^n) \rightarrow d^{n+} + d^{n-}$  will affect mainly the transition-metal sites. The change of the electron density at the intermediate oxygen site will be largely cancelled out.

to take into account only those contributions to the polarization function which are associated with the TM sites, and to suppress contributions associated with intermediate sites. This makes some difference from the conventional RPA,<sup>37,38,39</sup> which constitutes the basis of the GW method.<sup>43,44</sup> We expect this scheme to work well for the on-site Coulomb interactions. However, the effect of hybridization on the intersite Coulomb interactions remain an open and so far unresolved problem. Some estimates of these effects will be given in Sec. V IID, using the c-LDA method. The calculations suggest that the intersite interactions are screened very efficiently by the change of hybridization. Therefore we speculate that for the considered compounds, the effective Coulomb interactions between different TM sites are small and can be neglected.

The analytical expression for  $P^H$  can be obtained from Eq. (27) by considering the perturbation-theory expansion for the wavefunctions with the fixed occupation numbers.<sup>40</sup> The time-dependent perturbation theory, corresponding to the external perturbation  $V_{\text{ext}} e^{i\omega t}$ , yields in the first order:

$$P^H(\omega) = \sum_{ij} \frac{(n_i - n_j) d_{ij}^y d_{ji}^y}{i\omega + \epsilon_j - \epsilon_i + i0^+ (n_i - n_j)}; \quad (29)$$

where  $d_{ij} = \langle \psi_j | \psi_i \rangle$  is the projection of LDA eigenstate  $\psi_i$  onto one of partial d-waves  $\psi_j$ , belonging to the TM site, and  $i$  and  $j$  are the joint index, incorporating spin and band indices as well as the position of  $k$ -point in the first Brillouin zone. In this notation, the matrix multiplication in Eq. 28 implies the convolution over two indices. Namely, the matrix element of the product  $\hat{u} P^H$  is given by  $(\hat{u} P^H)_i = \sum_u u_{iu} P^H_u$ . Note that all transitions in Eq. (29) are allowed only between occupied and empty bands.

In the next Sections, we will discuss different contributions to the screening of Coulomb interactions more in details.

## B. Results of Constraint-LDA Calculations

The results of conventional constraint-LDA calculations for TM oxides have been widely discussed in the literature.<sup>3,27,28,30,31</sup> Here we only illustrate the main idea and show some basic results using  $\text{SrVO}_3$  as an example.

The calculations are performed in the supercell geometry, in which the number of atomic 3d electrons is modulated around the "ground-state" value  $n=1$  according to the formula:

$$n_R = n + \delta n \cos(kR):$$

Corresponding values of interaction parameter  $u_k$ , calculated in several different points of the Brillouin zone, are listed in Table X. Then, we map  $u_k$  onto the model



TABLE X: The values of  $u_k$  (in eV) obtained in constraint-LDA calculations for  $\text{SrVO}_3$  in different points of the Brillouin zone:  $\Gamma = (0;0;0)$ ,  $X = (\pi/a)(1;0;0)$ ,  $M = (\pi/a)(1;1;0)$ , and  $R = (\pi/a)(1;1;1)$ . The right column shows the weights of these  $k$ -points used in the process of integration over the Brillouin zone.

$k$	$u_k$	$W_k$
$\Gamma$	0	0
$X$	10.6	3=7
$M$	9.9	3=7
$R$	9.5	1=7

$$u_k = u + \sum_{\mathbf{R}} \frac{v}{R} \cos(\mathbf{k} \cdot \mathbf{R});$$

and extract parameters of on-site ( $u$ ) and NN ( $v$ ) interactions after integration over the Brillouin zone. We note that in the present context the  $\Gamma$ -point result has no physical meaning, as it corresponds to the transfer of an electron to the same atomic site. Therefore, we exclude it in the process of integration, and recalculate the weights of other  $k$ -points using the symmetry arguments. The new weights are shown in Table X. This yields the following parameters:  $u = 10.1$  eV and  $v = 1.2$  eV. Similar calculations for intra-atomic exchange coupling yield  $j = 1.0$  eV.

For comparison, the values of bare Coulomb and exchange integrals, calculated on the atomic V (3d) wavefunctions are 21.7 and 1.2 eV, respectively. Thus, in the c-LDA scheme the effective Coulomb interaction is reduced by factor two. The intra-atomic exchange interaction is reduced by 20%. As we will see in the next section, the Coulomb interaction will be further reduced by relaxation of the WF's due the change of hybridization.

### C. The Role of Hybridization

Because of hybridization, the d-states of the TM sites may have a significant weight in other bands. A typical situation for the series of TM oxides is shown in Fig. 1, where besides the  $t_{2g}$ -band, the d-states contribute to the TM  $e_g$  as well as the O (2p) bands. On both sides of the reaction  $2(d^n) \rightarrow d^{n+1} + d^{n-1}$ , the WF's constructed for the  $t_{2g}$  bands should be orthogonal to other bands. As it was already pointed out in Sec. V IIA, this mechanism is responsible for an additional channel of screening of the on-site Coulomb interaction associated with the change of this hybridization. The corresponding contribution can be evaluated using the Dyson equation (28) and taking the matrix of Coulomb interactions  $\hat{U}$  obtained in c-LDA as the starting interaction. Then, the relevant expression for the polarization matrix is given by Eq. (29).

According to the electronic structure of the TM oxides, one can identify three main contributions to the polarization matrix  $\hat{P}^H$ , associated with the following inter-band transitions: O (2p)  $\rightarrow$  TM ( $e_g$ ), O (2p)  $\rightarrow$  TM ( $t_{2g}$ ), and TM ( $t_{2g}$ )  $\rightarrow$  TM ( $e_g$ ). Meanwhile, all transitions between  $t_{2g}$  bands should be switched off, in order to avoid the double counting of these effects in the process of solution of the Hubbard model.<sup>39</sup> As it was already pointed out in Sec. V II, this procedure is similar to the setting  $\hat{H} = \hat{C}$  for the auxiliary WF's.

Details of static screening, corresponding to  $\omega = 0$ , are explained in Fig. 19 for  $\text{SrVO}_3$ . It is convenient to introduce three Kanamori parameters:<sup>46</sup> the intra-orbital Coulomb interaction  $U = U_{xy \uparrow xy \uparrow xy \downarrow xy \downarrow}$ , the inter-orbital interaction  $U^0 = U_{xy \uparrow xy \downarrow yz \uparrow yz \downarrow}$ , and the off-diagonal (exchange-type) interaction  $J = U_{xy \uparrow yz \downarrow xy \downarrow yz \uparrow}$ . In addition to the total value of  $U$ , we calculate intermediate interactions corresponding to each type of transitions in the polarization matrix (and neglecting the other two). The screening caused by the change of the hybridization appears to be very efficient. So, by going from c-LDA to RPA the intra-orbital interaction  $U$  is reduced from 11.2 to 2.5 eV (i.e., by factor four and even more). The main contribution to this screening comes from the O (2p)  $\rightarrow$  V ( $e_g$ ) and O (2p)  $\rightarrow$  V ( $t_{2g}$ ) transitions in the polarization functions. In the cubic perovskites, the direct interaction between V ( $t_{2g}$ ) and V ( $e_g$ ) bands plays a minor role and can be neglected.

Matrix elements of the (total) polarization function are displayed in Fig. 20. The largest contribution comes from the site-diagonal elements of the type  $P(\mathbf{l}) \rightarrow P^H(\mathbf{l}) = P^H(\mathbf{l})$ . Other contributions are considerably smaller. The static polarization  $P = P(0)$  is about  $0.12 \text{ eV}^{-1}$ . This is the large value because the renormalization of the on-site Coulomb interaction in the multi-orbital systems is controlled by the parameter  $M/P$ , rather than  $P$  (see Appendix). The prefactor  $M$  stands for the total number of orbitals per one TM site ( $M = 3$  for  $t_{2g}$  systems). Therefore,  $u/M/P$  can be estimated as 3.6, and the situation appears to be close to the strong-coupling regime. Then, the effective interaction is not sensitive to the exact value of the parameter  $u$ , which is used as the starting point in RPA calculations. For example, had we started with the bare Coulomb interaction, which exceed the c-LDA value by factor two and even

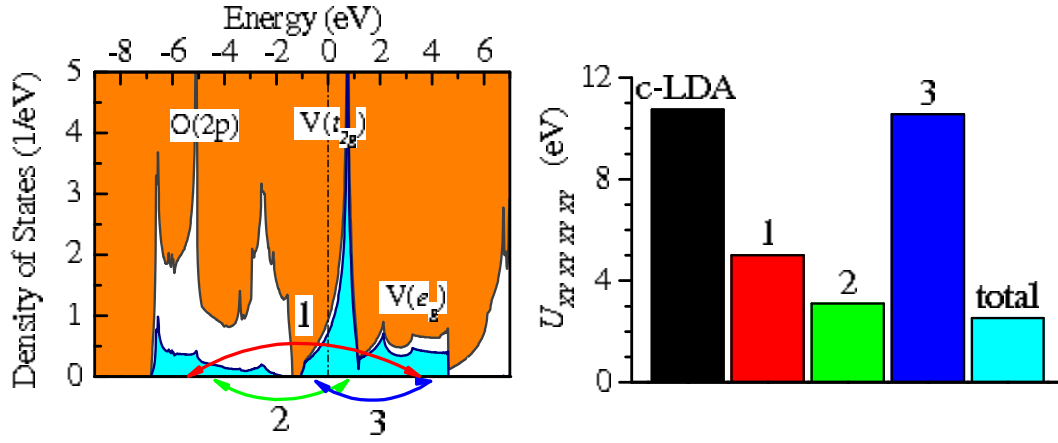


FIG. 19: Left panel shows the local density of states of  $\text{SrVO}_3$  with the notation of the main inter-band transitions which contribute to the polarization function in RPA:  $\text{O}(2p) \rightarrow \text{V}(e_g)$  (1),  $\text{O}(2p) \rightarrow \text{V}(t_{2g})$  (2), and  $\text{V}(t_{2g}) \rightarrow \text{V}(e_g)$  (3). Right panel shows the intra-orbital interaction  $U$  in c-LDA ( $U = U + \frac{8}{7}J$ ),<sup>45</sup> the effect of screening corresponding to each type of transitions in the polarization function, and the final value of  $U$  in RPA which incorporates all three transitions. All RPA results are for  $\epsilon = 0$ .

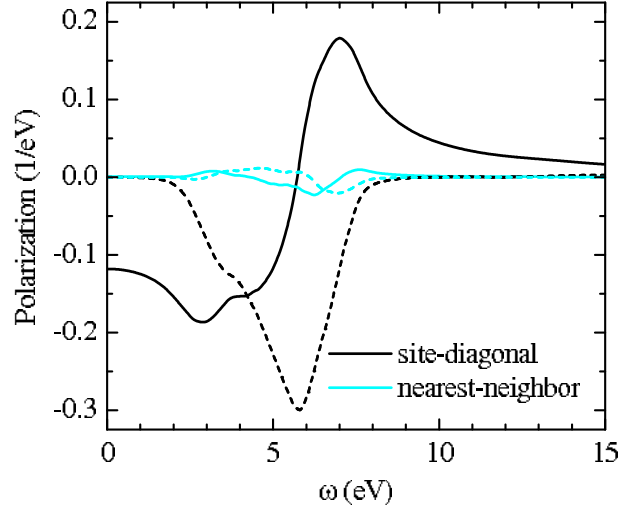


FIG. 20: The diagonal matrix element  $P_{xy,xy,xy,xy}^H$  of the polarization function for  $\text{SrVO}_3$  in the real space: the black curve shows the site-diagonal part, the light blue curve shows nearest-neighbor elements in the  $xy$ -plane. The real and imaginary parts are shown by solid and dashed curves, respectively.

more, we would have obtained  $U = 2.7$  eV, which is close to 2.5 eV derived by starting with c-LDA. This justifies some approximations discussed in Sec. V IIA, particularly the use of fast but not extremely accurate c-LDA for some channels of screening.

#### D. RPA versus Constraint-LDA for $t_{2g}$ Electrons

In this section we briefly return to the problem considered in Ref. 35 and reinterpret some results obtained in that work in the light of present RPA approach. The basic idea of Ref. 35 was to evaluate the effective Coulomb interaction for the series of TM perovskite oxides in the framework of c-LDA, which would incorporate the screening by itinerant TM ( $e_g$ ) electrons. Since for the considered type of screening, RPA has many similarities with c-LDA, the present section can be also regarded as a test for these two approaches.

However, it is important to remember that several basic assumptions of Ref. 35 were different from the present work.

So, the TM ( $t_{2g}$ ) states in Ref. 35 were totally decoupled from the rest of the electronic states by switching off the matrix elements of hybridization in the LMTO method, and only the TM ( $e_g$ ) states were allowed to hybridize. The corresponding electronic structure of  $\text{SrVO}_3$  is shown in Fig. 21. In terms of RPA polarization function, this means

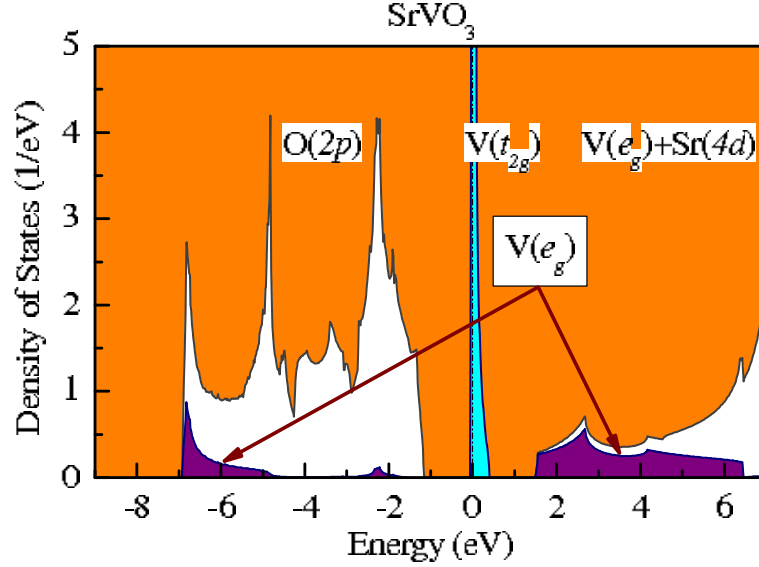


FIG. 21: Electronic structure of  $\text{SrVO}_3$  in canonical-bands approximation for the  $V(t_{2g})$  states.<sup>10</sup> the contributions of  $V(e_g)$  states are shown by arrows. Other notations are the same as in Fig. 1.

that the only allowed contributions to the screening in Ref. 35 were due to the  $O(2p) \rightarrow V(e_g)$  inter-band transitions (type 1 in Fig. 19).

Results of such c-LDA calculations for  $\text{SrVO}_3$ , which have been performed along the same line as in Sec. V IIB, are summarized in Table XI. After the Fourier transformation to the real space, we obtain the following parameters

TABLE XI: Results of constraint-LDA calculations for  $U_k$  between  $t_{2g}$  states in  $\text{SrVO}_3$  obtained after including the  $e_g$  states to the screening of  $t_{2g}$  interactions. Other notations are the same as in Table X.

$k$	$U_k$	$w_k$
		0
X	3.9	3=7
M	3.2	3=7
R	2.9	1=7

of on-site and NN interactions:  $U = 3.4$  eV and  $V = 0.3$  eV. This value of  $U$  appears to be in a reasonable agreement with the value  $U = 2.5$  eV, extracted from RPA (Fig. 19). However, c-LDA employs an additional atomic-spheres approximation. Therefore, for a proper comparison with RPA, one should use the same level of approximation and suppress all nonspherical interactions in the matrix of Coulomb interactions  $\hat{u}$ , which is used as the starting point in RPA. In this approximation, and considering only the  $O(2p) \rightarrow V(e_g)$  transitions in the polarization function, we obtain  $U = 3.6$  eV, which is close to the c-LDA value obtained using the method proposed in Ref. 35. The small difference is caused by different approximations used for treating the intersite Coulomb interactions, which were neglected in RPA and taken into account in c-LDA. For comparison, the total value of  $U$  obtained in RPA after neglecting the nonsphericity effects is only 1.6 eV.

In summarizing this section, there is a reasonable agreement between results of RPA calculations and the c-LDA approach proposed in Ref. 35. However, the agreement is somewhat fortuitous because this c-LDA takes into account only one part of the total screening, corresponding to the  $O(2p) \rightarrow V(e_g)$  transitions in the polarization function. The error caused by this approximation is partially compensated by the atomic-spheres approximation supplementing the c-LDA scheme.

The c-LDA calculations give some idea about the effect of hybridization on the screening of intersite Coulomb interactions. The screening appears to be very efficient. So, by taking into account only the  $O(2p) \rightarrow V(e_g)$  transitions,

the NN interaction is reduced from 1.2 to 0.3 eV. We expect this value to be further reduced by including other types of transitions in the polarization function. Thus, for the considered compounds, the effective Coulomb interaction between different TM sites seems to be small and can be neglected.

#### E. Doping-Dependence and Kanamori Rules for Cubic Compounds

In this section we discuss the effects of electron/hole doping on the static Coulomb interactions in  $\text{SrVO}_3$  using the rigid-band approximation. Results of such c-LDA+RPA calculations are shown in Fig. 22 versus the total number of electrons in the TM ( $t_{2g}$ ) band,  $n_{t_{2g}}$ . We monitor the behavior of three Kanamori parameters:<sup>46</sup>  $U$ ,  $U^0$ , and  $J$ .

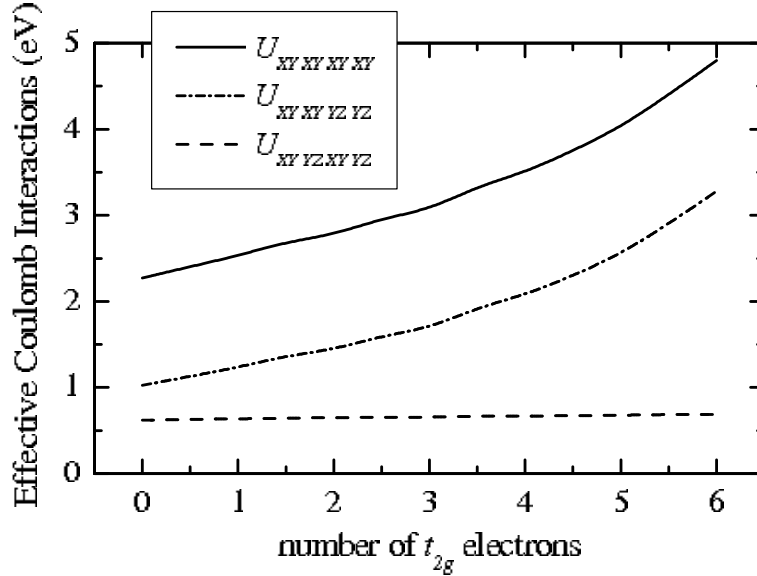


FIG. 22: Doping-dependence of the effective Coulomb interactions in  $\text{SrVO}_3$ .

The Coulomb interactions reveal a monotonic behavior as the function of doping. The screening is the most efficient when the  $t_{2g}$  band is empty ( $n_{t_{2g}} = 0$ ). The situation corresponds to  $\text{SrTiO}_3$ . In this case all  $O(2p)$  TM ( $t_{2g}$ ) transitions contribute to the screening in RPA (see Fig. 19). This channel of screening vanishes when the  $t_{2g}$  band becomes occupied ( $n_{t_{2g}} = 6$ ). Then, the only possible screening is associated with the  $O(2p)$  TM ( $e_g$ ) transitions in the polarization function, and the effective Coulomb interaction becomes large.

The screening of off-diagonal matrix element  $J$  practically does not depend on doping. Therefore, the well known Kanamori rule,  $U = U^0 + 2J$ , which was originally established for atoms, works well in the cubic compounds, even after the screening of  $t_{2g}$  interactions by other electrons.

The present result also supports an old empirical rule suggesting that only the Coulomb integral  $U$  is sensitive to the crystal environment in solids. The nonspherical interactions, which are responsible for Hund's first and second rules, appears to be much closer to their atomic values.<sup>34,47</sup>

#### F. Frequency-Dependence

We have shown that the change of hybridization plays a very important role and strongly reduces the static value of  $U$ . However, this is only one part of the story because the same effect implies the strong frequency-dependence of the effective interaction, as it immediately follows from the Kramers-Kronig transformation in RPA:<sup>44</sup>

$$\text{Re} \hat{U}(\omega) = \hat{U} - \frac{2}{\pi} \text{P} \int_0^{\infty} d\omega' \frac{\omega' \text{Im} \hat{U}(\omega')}{\omega'^2 - \omega^2} \quad (30)$$

Indeed, the difference  $[\hat{U} - \text{Re} \hat{U}(\omega)]$  at  $\omega = 0$ , which for the diagonal matrix elements of  $\text{SrVO}_3$  is about 8.7 eV, should be related with the existence of the finite spectral weight of  $\text{Im} \hat{U}(\omega)$  at finite  $\omega$ . These dependencies are shown in Fig. 23 for  $\text{SrVO}_3$ .

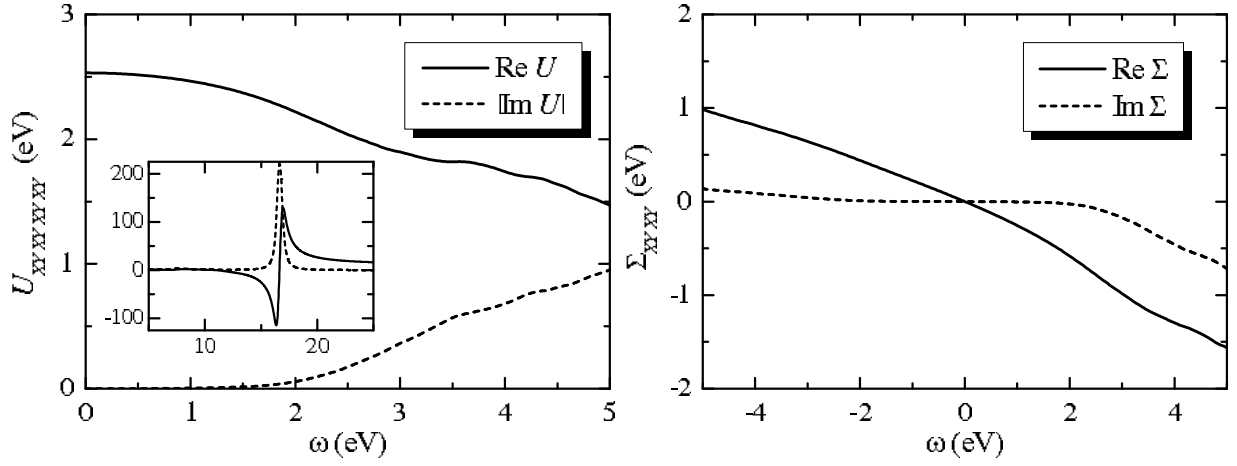


FIG. 23: Frequency dependence of diagonal matrix elements of screened Coulomb interaction (left) and self-energy obtained in the GW scheme for  $\text{SrVO}_3$ . The inset shows the high-frequency part of  $U$ .

The high-frequency part of  $\hat{U}$  can also contribute to the low-energy part of the spectrum through the self-energy effect.<sup>39</sup> The latter can be evaluated in the GW approximation,<sup>43,44</sup> where the self-energy is given by the convolution of  $\hat{U}(\omega)$  with the one-particle Green function  $\hat{G}(\omega)$  for the  $t_{2g}$  band:

$$\hat{G}(\omega) = \frac{i}{2} \sum_{\omega'} \hat{G}(\omega') \hat{U}(\omega - \omega').$$

For  $\text{SrVO}_3$ , the diagonal matrix element of  $\hat{G}(\omega)$  is also shown in Fig. 23. The low-frequency part of  $\text{Im } \hat{G}$  is small and can be neglected, while  $\text{Re } \hat{G}$  mainly contributes to the renormalization factor:

$$Z = 1 - \partial \text{Re } \hat{G} / \partial \omega|_{\omega=0}^{-1}.$$

The latter is estimated as 0.8, for the diagonal matrix elements.

#### G. Lattice Distortion, Formal Valency and Screening

In Sec. VIB we already pointed out that the degree of hybridization between atomic TM ( $t_{2g}$ ) and O (2p) states can differ substantially for different TM oxides. A typical example is two isoelectronic perovskites:  $\text{SrVO}_3$  and  $\text{YTiO}_3$ . The TM ( $t_{2g}$ )-O (2p) hybridization is stronger in  $\text{SrVO}_3$ , because of two reasons:

- (i) A direct proximity of O (2p) and V ( $t_{2g}$ ) bands in  $\text{SrVO}_3$ , which is expected for tetra-valent compounds;
- (ii) A strong orthorhombic distortion observed in  $\text{YTiO}_3$ , which generally deteriorates the Ti( $t_{2g}$ )-O (2p) hybridization.

Therefore, it is reasonable to expect a very different screening of on-site Coulomb interactions in these two compounds. This idea is nicely supported by results of RPA calculations shown in Fig. 24. The static  $U$  is larger in  $\text{YTiO}_3$ . For example, the diagonal matrix element of  $\hat{U}$  is about 3.4 eV, against 2.5 eV in  $\text{SrVO}_3$ . This is despite the fact that c-LDA has an opposite tendency. Generally, the value of  $U$  in c-LDA is expected to be larger for  $\text{SrVO}_3$  rather than for  $\text{YTiO}_3$ , due to different shape of the atomic 3d-wavefunctions in the three- and tetra-valent compounds.<sup>33</sup> So, c-LDA yields  $U = 8.9$  and  $10.1$  eV, correspondingly for  $\text{YTiO}_3$  and  $\text{SrVO}_3$ . These parameters have been used as the starting point in RPA, which results in an opposite trend for the static  $U$ .

Therefore, the RPA screening is more efficient in  $\text{SrVO}_3$ , which is consistent with stronger TM ( $t_{2g}$ )-O (2p) hybridization in this compound. On the other hand, the frequency-dependence of  $\hat{U}$  is weaker in  $\text{YTiO}_3$ , as it immediately follows from the Kramers-Kronig transformation (30).

Finally, because of different hybridization of the  $t_{2g}$  orbitals in  $\text{YTiO}_3$ , the diagonal matrix elements of  $\hat{U}$  are also different (see Fig. 24). In this case, there is some deviation from the Kanamori rules. The difference is small (about 0.07 eV for diagonal matrix elements of  $\hat{U}$  at  $\omega = 0$ ). However, it may play some role in more delicate applications, such as the orbital magnetism in solids, for example.<sup>34</sup>

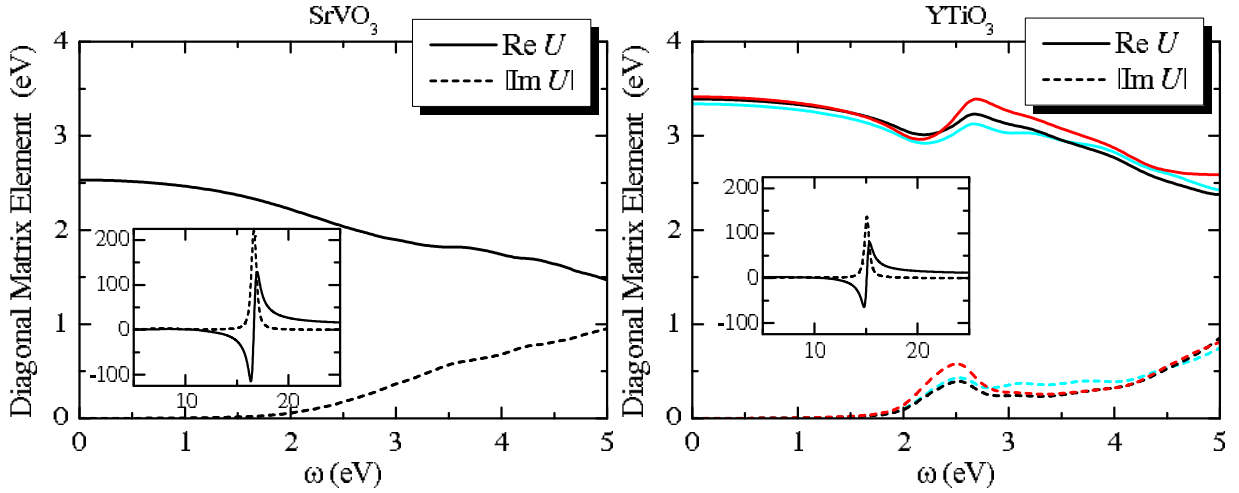


FIG. 24: Diagonal matrix elements of screened Coulomb interactions for  $\text{SrVO}_3$  (left) and  $\text{YTiO}_3$  (right). Three different lines in the case of  $\text{YTiO}_3$  show the behavior of three diagonal matrix elements in the local coordinate frame given by Eq. (20). The insets show the high-frequency part of  $\hat{U}$ . The lines corresponding to different  $t_{2g}$  orbitals in the case of  $\text{YTiO}_3$  are indistinguishably close.

#### H. Two Models for $\text{V}_2\text{O}_3$

In Sec. V ID we introduced two possible models for the kinetic-energy part of  $\text{V}_2\text{O}_3$ : the “*ve-orbital model*” treats all V (3d) bands on an equal footing, while the “*three-orbital model*” is limited by twelve V ( $t_{2g}$ ) bands, close to the Fermi level. We argued that parameters of the kinetic energy can be different for these two models. The same is true for the effective Coulomb interactions. The RPA provides a very transparent explanation for this difference, which is based on the following arguments. Recall that RPA incorporates the screening of on-site Coulomb interactions caused by relaxation of the wavefunctions. This relaxation is treated analytically, using regular perturbation theory for the wavefunctions, which results in Eq. (29) for the polarization function.<sup>40</sup>

Since the V ( $e_g$ ) band is eliminated in the three-orbital model, the effective  $\hat{U}$  should include the screening caused by that change of the wavefunctions, which is formulated in terms of transitions between V ( $t_{2g}$ ) and V ( $e_g$ ) bands in the perturbation-theory expansion. In the *ve-orbital model*, the V ( $e_g$ ) band is included explicitly. Therefore, the relaxation caused by possible interactions between V ( $t_{2g}$ ) and V ( $e_g$ ) bands will be automatically taken into account in the process of solution of the *ve-orbital model*, and we should get rid of this parasitic screening at the stage the construction of the model Hamiltonian. Thus, the *three-orbital model* will include an additional screening of on-site interactions, caused by the V ( $t_{2g}$ )! V ( $e_g$ ) transitions in the polarization function, which does not appear in the *ve-orbital model*.

This screening appears to be rather efficient (unlike in cubic perovskites considered in Sec. V IIC). So, the diagonal matrix element of static  $t_{2g}$  interactions is about 3.2 and 3.9 eV, for the three- and *ve-orbital model*, respectively (Fig. 25). On the other hand, according to the Kramers-Kronig transformation (30), the frequency-dependence of the effective interaction is more important in the three-orbital model. Because of different hybridization of  $t_{2g}$  and  $e_g$  states in the *ve-orbital model*, the  $e_g$  interactions are screened more efficiently (the static interaction between  $e_g$  orbitals is about 3.7 eV).

### VIII. SUMMARY, OPEN QUESTIONS, AND COMPARISON WITH OTHER METHODS

The ultimate goal of this work was to make a bridge between first-principle electronic structure calculations and the universe of Hubbard parameters for strongly-correlated systems. We have presented a comprehensive analysis of the problem, by starting with the brief description of the ASA-LMTO method for electronic structure calculations and ending up with realistic parameters of the kinetic energy and the Coulomb interactions for the series of TM oxides obtained on the basis of this LMTO method. A particular attention has been paid to the analysis of microscopic processes responsible for the screening of on-site Coulomb interactions in oxide compounds.

Our strategy consists of three steps:

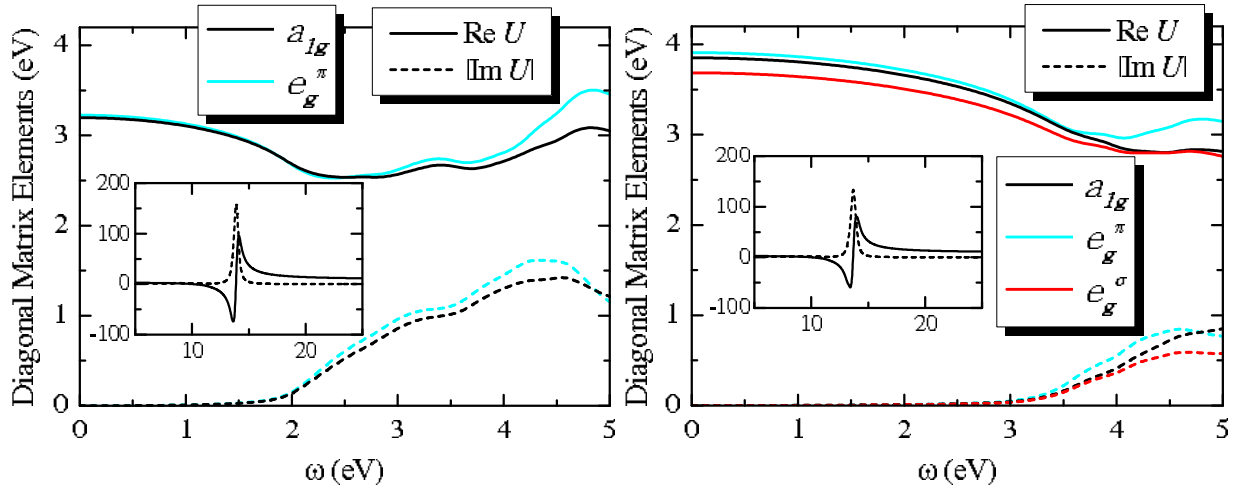


FIG. 25: Diagonal matrix elements of screened Coulomb interactions obtained in the three- (left) and five- (right) orbital models for  $V_2O_3$ . The notations of orbitals are given in Sec. V D. Other notations are the same as in Fig. 24.

(i) Derivation of the kinetic-energy part of the Hubbard model from the single-particle electronic structure in LDA, using the downfolding method. We have also considered corrections to the crystal-field splitting caused by nonsphericity of electron-ion interactions, beyond the conventional atomic-spheres-approximation.

(ii) Construction of the Wannier functions using results of the downfolding method. At this stage we closely follow the idea of LMTO method, and construct the WFs as the LMTO basis functions, which after applying to the Kohn-Sham Hamiltonian in the real space generate the matrix elements of the kinetic energy obtained in the downfolding method.

(iii) Calculation of screened Coulomb interactions using the concept of auxiliary WFs. The latter are defined as the Wannier orbitals for which the kinetic-energy part is set to be zero. This construction allows to avoid the double counting of the kinetic-energy term, which is included explicitly in the Hubbard model. The screened Coulomb interactions are calculated on the basis of a hybrid approach, combining the conventional constraint-LDA with the random-phase approximation for treating the hybridization effects between atomic TM (3d) and O (2p) orbitals. The latter play a very important role and yields a strong renormalization of the effective Coulomb interaction for isolated  $t_{2g}$  band. It also explains a strong material-dependence of this interaction, which is sensitive to the crystal environment in solids, the number of  $t_{2g}$  electrons, the valent state of the TM ions, etc.

Taking into account a wide interest to the construction of effective lattice fermion models from the first principles, we would like to make a brief comparison with other works on a similar subject.

Majority of methods start with the construction of the WFs, which are then used as the basis for calculations of the parameters of the kinetic energy and the Coulomb interactions. This is different from our approach, where we start with the kinetic-energy part, and only after that construct the WFs for a given set of parameters of the kinetic energy. We believe that such an order is extremely important, as it allows us to control the contributions of the kinetic energy to the WFs and the Coulomb interactions.

Among recent works, a considerable attention is paid to the method of Marzari and Vanderbilt, because it allows to control the spacial extension of the WFs. Very recently, Schnell et al. applied this method to calculations of the parameters of the Hubbard Hamiltonian for the series of 3d transition metals.<sup>48</sup> In each  $k$ -point of the Brillouin zone, they constructed the WFs from all 16 bands of the LDA Hamiltonian, corresponding to the 4s4p3d4f LMTO basis. Therefore, the total number of Wannier orbitals was also 16. The coefficients of this expansion has been chosen so to minimize the square of the position operator,  $\langle r^2 \rangle = \langle W | j^2 | W \rangle$ . The obtained WFs were indeed well localized, and the parameter  $U$  estimated for the 3d bands was very close to the atomic value (about 25 eV). However, the corresponding Wannier basis set is too large, that does not make a big difference from the original LMTO basis set, for which one can also introduce a localized (tight-binding) representation.<sup>10</sup> From the view point of numerical solution of the Hubbard model using modern many-body techniques, it is still hardly feasible to work in the basis of 16 Wannier orbitals per one TM site, while the simplest Hartree-Fock approximation is definitely not sufficient for the transition metals.<sup>48</sup> It would be interesting to see how this method will work for the TM oxides, considered in the present work, where the physical basis set is limited by three Wannier orbitals per one TM site. For example, is it possible to construct the localized Wannier orbitals for isolated  $t_{2g}$  bands in the TM oxides, which would be as good as the Wannier orbitals derived for all bands? The problem is that when the number of bands decreases, the number of variational parameters for the optimization of the Wannier orbitals will also decreases. Therefore, the Wannier orbitals will generally become

less localized, as it was demonstrated in our work for  $V_2O_3$ . Also, when the problem is formulated in a reduced Hilbert space of bands closest to the Fermi level, it is very important to consider the screening of Coulomb interactions by other bands, which comes from relaxation of the wavefunctions. These effects are beyond the scopes of the work of Schnell et al., who only considered the bare Coulomb interactions.

In order to construct the WFs, Ku et al. employed the projector-operator scheme,<sup>49</sup> which is basically the initial step of the method of Marzari and Vanderbilt, prior the optimization.<sup>13</sup> In this scheme, each Wannier orbital is generated by projecting a trial wavefunction,  $\tilde{\psi}_i$ , onto a chosen subset of bands (in our case,  $t_{2g}$  bands):

$$\tilde{W}_i = \sum_{j \in t_{2g}} \langle j | \tilde{\psi}_i \rangle \tilde{\psi}_j$$

Since such orbitals are not orthonormal, the procedure is followed by the numerical orthonormalization, similar to the one described in Sec. II. These WFs have been used as the basis for the construction of the low-energy Hamiltonian for the series of cuprates, like  $La_4Ba_2Cu_2O_{10}$ , where the Wannier basis consisted of a single orbital centered around each Cu site. A weak point of this approach is that it is difficult to assess the spacial extension of the WF, which crucially depends on the trial wavefunction, and can be affected by the orthonormalization. In some sense, the result strongly depends on authors' intuition on how they choose the trial wavefunction. For example, the bare Coulomb interaction obtained in Ref. 49 in the basis of their WFs was only 7.5 eV, which is much smaller than the atomic Coulomb integral for the Cu (3d) orbitals. This means that the WFs are not well localized. It is not clear at present, whether this is a result of the bad choice of the trial wavefunction, or there is a more fundamental problem related with the fact that a more compact representation for the WFs simply may not exist in this case. Note, that apart from the Berry phase, there is no further parameters available for the optimization of the WFs in the single-orbital case.

The delocalization of the WFs gives rise to appreciable direct exchange interactions operating between different Cu sites.<sup>49</sup> This result, however, rises additional questions. Note, that the kinetic part of the Hubbard model and the WFs are evaluated in LDA, where the exchange-correlation potential is set to be local. In principle, non-local effects can be already incorporated in LDA, through the renormalization of parameters of the kinetic energy and the local interactions.<sup>50</sup> Therefore, it is not clear whether the nonlocal exchange interactions should be regarded as independent parameters of the Hubbard Hamiltonian or not.

Finally, Ku et al. calculated only bare Coulomb interactions. They did not consider the screening of these interactions caused by relaxation effects, which are extremely important.

Anisimov et. al. employed a similar approach for the analysis of spectroscopic properties of TM oxides.<sup>51</sup> They extracted only the kinetic-energy part of the Hubbard Hamiltonian, using the WFs constructed in the LMTO basis, and treated the Coulomb interaction  $U$  as a parameter.

A completely different strategy has been proposed by Andersen et. al., on the basis of their order- $N$  mu-ntin orbital (NMTOM) method, which is an extension of the LMTO method.<sup>52</sup> From the very beginning, they construct the NMTOM basis functions in certain energy interval as the WFs of the original KS Hamiltonian. Pavarini et al. applied this method to the series of  $d^1$  perovskites.<sup>53</sup> At present, it is not clear how the nonuniqueness of the WFs is reflected in the construction of the NMTOM basis set. Obviously, such a basis set is also not unique, and there is some freedom left for the localization of the Wannier orbitals, which does not seem to be well controlled. Generally, our transfer integrals for the  $d^1$  perovskites seem to be more localized and our crystal-field splitting is smaller. For example, had we relaxed the constraint condition for the construction of the "heads" of the WFs, based on the diagonalization of the density matrix (19), our conclusion would have been also different: the crystal-field splitting would increase, but the transfer integrals would become less localized.

Pavarini et al. did not calculate the Coulomb interactions. Instead, they used  $U = 5$  eV as a parameter, with the reference to the photoemission data.<sup>54</sup> However, the photoemission data are typically interpreted in the cluster model, which treats the O (2p) band explicitly. For the isolated  $t_{2g}$  band, the effective interaction should include an additional renormalization coming from the relaxation of the O (2p) band, which is eliminated in the  $t_{2g}$ -model. Therefore, the value of the effective  $U$  should be smaller.

Finally, due to unknown for us reason, there is a substantial difference of the parameters of  $t_{2g}$  bandwidth ( $W_{t_{2g}}$ ) between our work and Ref. 53, even for cubic  $SrVO_3$ . The parameters reported by Pavarini et al. are generally overestimated by about 30%.<sup>55</sup> Our conclusions about magnetic properties of  $YTiO_3$  and  $LaTiO_3$  are also different.<sup>11</sup> Details will be presented in a separate paper.

#### Acknowledgments

I thank Professor Masatoshi Imada for valuable suggestions, especially for drawing my attention to the problem of Wannier functions, nonsphericity of electron-ion interactions and its effect on the crystal-field splitting,<sup>12</sup> and the random-phase approximation for calculating the effective interaction parameters in the Hubbard model.<sup>39</sup>



## APPENDIX A : ORBITAL DEGENERACY AND SCREENING IN RPA

In this Appendix we consider the screening of on-site Coulomb interactions in RPA for an  $M$ -orbital system. All orbitals are supposed to be equivalent. For simplicity we neglect small nonsphericity of bare Coulomb interactions. Then, the nonvanishing matrix elements of the Coulomb interactions are  $u_{\alpha\alpha}$ , where  $\alpha = 1; \dots; M$ . They can be presented in the form  $\hat{u} = u\hat{I}$ , where  $\hat{I}$  is the  $M \times M$  matrix, consisting of only the units:

$$\hat{I} = \begin{pmatrix} 0 & 1 & 1 & & 1 & 1 \\ 1 & 1 & & & & \\ 1 & & 1 & & & \\ \vdots & & & \ddots & & \\ 1 & & & & 1 & \\ & & & & & 1 \end{pmatrix}$$

The part of the polarization matrix (29), which can interact with the matrix  $\hat{u}$ , is assumed to be diagonal:  $P_{\alpha\alpha} = P$ . The assumption is justified for cubic perovskites, where different  $t_{2g}$  orbitals belong to different bands. For other compounds it can be regarded as an approximation, which does not change our qualitative conclusion. Hence, for the screened Coulomb interaction (28) we have:

$$\hat{U} = [1 - \hat{u}P]^{-1} \hat{u} = \sum_{n=0}^{\infty} (uP)^n \hat{I}^n u\hat{I} \quad (\text{A } 1)$$

Since  $\hat{I}^{n+1} = M^{-1} \hat{I}^n$ , Eq. (A 1) can be converted to

$$\hat{U} = \sum_{n=0}^{\infty} (uMP)^n u\hat{I} = \frac{u}{1 - uMP} \hat{I}$$

This means that in the multi-orbital systems, the renormalization of the Coulomb repulsion is more efficient as it is controlled by the quantity  $(MP)$ , where the prefactor  $M$  stands for the number of orbitals.

In the strong coupling limit,  $uMP \gg 1$ , the effective interaction is  $\hat{U} = (MP)^{-1} \hat{I}$ , which does not depend on the value of bare Coulomb interaction  $u$ .

Electronic address: solovyev.igor@nim.sgo.jp; Present address: Computational Materials Science Center (CMSC), National Institute for Materials Science (NIMS), 1-2-1 Sengen, Tsukuba, Ibaraki 305-0047, Japan

- <sup>1</sup> P. Hohenberg and W. Kohn, Phys. Rev. 136, B864 (1964).
- <sup>2</sup> W. Kohn and L. J. Sham, Phys. Rev. 140, A1133 (1965).
- <sup>3</sup> V. I. Anisimov, J. Zaanen, and O. K. Andersen, Phys. Rev. B 44, 943 (1991).
- <sup>4</sup> V. I. Anisimov, F. Aryasetiawan, and A. I. Lichtenstein, J. Phys. Condens. Matter 9, 767 (1997).
- <sup>5</sup> M. Imada, A. Fujimori, and Y. Tokura, Rev. Mod. Phys. 70, 1039 (1998).
- <sup>6</sup> I. V. Solovyev, in Recent Research Developments in Magnetism and Magnetic Materials (Transworld Research Network, India, 2003), Vol. 1, pp. 253-294.
- <sup>7</sup> I. V. Solovyev, P. H. Dederichs, and V. I. Anisimov, Phys. Rev. B 50, 16861 (1994).
- <sup>8</sup> V. I. Anisimov, A. I. Poteryaev, M. A. Korotin, A. O. Anokhin, and G. Kotliar, J. Phys. Condens. Matter 9, 7359 (1997); S. Y. Savrasov, G. Kotliar, and E. Abraham, Nature 410, 793 (2001); K. Held, G. Keller, V. Eyert, D. Vollhardt, and V. I. Anisimov, Phys. Rev. Lett. 86, 5345 (2001); A. I. Lichtenstein, M. I. Katsnelson, and G. Kotliar, Phys. Rev. Lett. 87, 067205 (2001).
- <sup>9</sup> Y. Imai, I. V. Solovyev, and M. Imada, cond-mat/0503270.
- <sup>10</sup> O. K. Andersen, Phys. Rev. B 12, 3060 (1975); O. Gunnarsson, O. Jepsen, and O. K. Andersen, ibid. 27, 7144 (1983); O. K. Andersen and O. Jepsen, Phys. Rev. Lett. 53, 2571 (1984); O. K. Andersen, in The Electronic Structure of Complex Systems, ed. by P. Phariseau and W. M. Temmerman (Plenum Publishing Corporation, 1984); H. L. Skriver, The LMTO Method, (Springer-Verlag, Berlin, 1984); O. K. Andersen, Z. Pawłowska, and O. Jepsen, Phys. Rev. B 34, 5253 (1986); O. K. Andersen, O. Jepsen, and M. Sob, in Electronic Band Structure and Its Applications, ed. by M. Yussouf (Springer-Verlag, Berlin, 1986); homepage: <http://www.fkf.mpg.de/andersen/>.
- <sup>11</sup> I. V. Solovyev, Phys. Rev. B 69, 134403 (2004).
- <sup>12</sup> M. Mochizuki and M. Imada, Phys. Rev. Lett. 91, 167203 (2003).
- <sup>13</sup> N. Marzari and D. Vanderbilt, Phys. Rev. B 56, 12847 (1997).
- <sup>14</sup> C. J. Bradley and A. P. Cracknell, The Mathematical Theory of Symmetry in Solids (Clarendon Press, Oxford, 1972).

- 15 J. C. Slater and G. F. Koster, Phys. Rev. 94, 1498 (1954).
- 16 A. B. Harris, T. Yildirim, A. Aharony, O. Entin-Wohlman, and I. Korenblit, Phys. Rev. Lett. 91, 087206 (2003).
- 17 M. Posternak, A. Baldereschi, S. Massidda, and N. Mazari, Phys. Rev. B 65, 184422 (2002).
- 18 For example, one can construct the WFs simultaneously for the  $t_{2g}$  and O (2p) bands of  $\text{SrVO}_3$ , by starting with the V (3d- $t_{2g}$ ) and O (2p) orbitals (which form the t-part of the WFs) and including the V (3d- $e_g$ ) and Sr(4d5s) partial waves into the r-part, in order to enforce the orthogonality to other bands. In this case we do not need to worry about extension of the WFs centered at the V sites onto the oxygen sites because the O (2p) states are explicitly included into the Wannier basis. Hence, the WFs can be made more localized. Indeed, in this case we obtain  $\langle r^2 \rangle = 0.66$  and  $1.87 \text{ \AA}^2$  for the Wannier orbitals centered at the V and O sites, respectively. These values are already comparable with those obtained in Ref. 17 for  $\text{MnO}$ , using the procedure of Mazari and Vanderbilt.
- 19 Note that this splitting is different from the "two-down, one-up" scheme of the atomic  $t_{2g}$  levels (0.069, 0.042, and 0.112 eV) reported in Ref. 11. The difference is related with nonsphericity of the electron-ion interaction which was not considered in Ref. 11. The new scheme of the crystal-field splitting tends to stabilize a single  $t_{2g}$  orbital and thereby suppress the orbital fluctuations. On the Hartree-Fock level, the magnetic ground state of  $\text{YTiO}_3$  and  $\text{LaTiO}_3$  is expected to be ferromagnetic and A-type antiferromagnetic, respectively, in agreement with Ref. 11. Other details will be reported in a separate paper.
- 20 I. V. Solovyev, Phys. Rev. B 67, 174406 (2003).
- 21 J. S. Gardner, B. D. Gaulin, S.-H. Lee, C. Broholm, N. P. Raju, and J. E. Greedan, Phys. Rev. Lett. 83, 211 (1999); C. H. Booth, J. S. Gardner, G. H. Kwei, R. H. Heuser, F. Bridges, and M. A. Subramanian, Phys. Rev. B 62, R755 (2000); A. Keren and J. S. Gardner, Phys. Rev. Lett. 87, 177201 (2001).
- 22 Y. Taguchi, Y. Ohara, H. Yoshizawa, N. Nagaosa, and Y. Tokura, Science 291, 2573 (2001).
- 23 S. Yonezawa, Y. Muraoka, Y. Matsushita, and Z. Hiroi, J. Phys. Soc. Jpn. 73, 819 (2004); Z. Hiroi, S. Yonezawa, and Y. Muraoka, ibid. 73, 1651 (2004).
- 24 D. B. McWhan, T. M. Rice, and J. P. Renfrew, Phys. Rev. Lett. 23, 1384 (1969).
- 25 S. Yu. Ezhov, V. I. Anisimov, D. I. Khomskii, and G. A. Sawatzky, Phys. Rev. Lett. 83, 4136 (1999); A. I. Poteryaev, A. I. Lichtenstein, and G. Kotliar, ibid. 93, 086401 (2004).
- 26 P. H. Dederichs, S. Blugel, R. Zeller, and H. Akai, Phys. Rev. Lett. 53, 2512 (1984).
- 27 M. Norman and A. Freeman, Phys. Rev. B 33, 8896 (1986).
- 28 A. K. M. Chahan, R. M. Martin, and S. Satpathy, Phys. Rev. B 38, 6650 (1988).
- 29 M. S. Hybertsen, M. Schluter, and N. E. Christensen, Phys. Rev. B 39, 9028 (1989).
- 30 O. Gunnarsson, O. K. Andersen, O. Jepsen, and J. Zaanen, Phys. Rev. B 39, 1708 (1989).
- 31 O. Gunnarsson, A. V. Postnikov, and O. K. Andersen, Phys. Rev. B 40, 10407 (1989).
- 32 V. I. Anisimov and O. Gunnarsson, Phys. Rev. B 43, 7570 (1991).
- 33 I. V. Solovyev and P. H. Dederichs, Phys. Rev. B 49, 6736 (1994).
- 34 M. Norman, Phys. Rev. B 52, 1421 (1995); M. S. Brooks, J. Phys. Condens. Matter 13, L469 (2001).
- 35 I. Solovyev, N. Hamada, and K. Terakura, Phys. Rev. B 53, 7158 (1996).
- 36 W. E. Pickett, S. C. Erwin, and E. C. Ethridge, Phys. Rev. B 58, 1201 (1998).
- 37 M. Springer and F. Aryasetiawan, Phys. Rev. B 57, 4364 (1998).
- 38 T. Kotani, J. Phys. Condens. Matter 12, 2413 (2000).
- 39 F. Aryasetiawan, M. Imada, A. Georges, G. Kotliar, S. Biermann, and A. I. Lichtenstein, Phys. Rev. B 70, 195104 (2004).
- 40 I. V. Solovyev and M. Imada, Phys. Rev. B 71, 045103 (2005).
- 41 C. Herring, in Magnetism, ed. by G. T. Rado and H. Suhl (Academic, New York, 1966), Vol. IV.
- 42 In the present work we employ the setting:  $\hat{W}^\dagger(\mathbf{C})\hat{H}_{KS}\hat{W}(\mathbf{C}) = E$
- 43 L. Hedin, Phys. Rev. 139, A796 (1965).
- 44 F. Aryasetiawan and O. Gunnarsson, Rep. Prog. Phys. 61, 237 (1998).
- 45 In the atomic limit, the  $5 \times 5 \times 5$  matrix of the Coulomb interactions between d electrons is totally specified by three radial Slater's integrals:  $F^0$ ,  $F^2$ , and  $F^4$ . Then, we use the following definitions for the parameters  $u$  and  $j$  in terms of  $F^0$ ,  $F^2$ , and  $F^4$ :  $u = F^0$  and  $j = \frac{1}{14}(F^2 + F^4)$ . In LDA+U, one can use the ratio:  $F^4 = F^2 \cdot 0.63$ , which holds in the atomic limit. It allows to obtain all three Slater's integrals, using the values of only two parameters,  $u$  and  $j$ , extracted from c-LDA. We also list here several useful identities which hold for Coulomb matrix elements between  $t_{2g}$  orbitals:  $u_{xy \uparrow xy \downarrow xy \downarrow} = F^0 + \frac{4}{49}F^2 + \frac{36}{441}F^4$  ( $u + \frac{8}{7}j$ ),  $u_{xy \uparrow xy \downarrow yz \uparrow} = F^0 - \frac{2}{49}F^2 - \frac{4}{441}F^4$ , and  $u_{xy \uparrow yz \uparrow yz \downarrow} = \frac{3}{49}F^2 + \frac{20}{441}F^4$ .
- 46 J. Kanamori, Prog. Theor. Phys. 30, 275 (1963).
- 47 D. van der Marel and G. A. Sawatzky, Phys. Rev. B 37, 10674 (1988).
- 48 I. Schnell, G. Czucholl, and R. C. Albers, Phys. Rev. B 65, 075103 (2002); I. Schnell, PhD Thesis (University of Bremen, Germany, 2002); I. Schnell, G. Czucholl, and R. C. Albers, Phys. Rev. B 68, 245102 (2002).
- 49 Wei Ku, H. Rosner, W. E. Pickett, and R. T. Scalettar, Phys. Rev. Lett. 89, 167204 (2002).
- 50 I. V. Solovyev, Phys. Rev. B 60, 8550 (1999).
- 51 V. I. Anisimov, D. E. Kondakov, A. V. Kozhevnikov, I. A. Nekrasov, Z. V. Pchelkina, J. W. Allen, S.-K. Mo, H.-D. Kim, P. Metcalfe, S. Suga, A. Sekiyama, G. Keller, I. Leonov, X. Ren, and D. Vollhardt, Phys. Rev. B 71, 125119 (2005).
- 52 O. K. Andersen and T. Saha-Dasgupta, Phys. Rev. B 62, R16219 (2000).
- 53 E. Pavarini, S. Biermann, A. Poteryaev, A. I. Lichtenstein, A. Georges, and O. K. Andersen, Phys. Rev. Lett. 92, 176403 (2004); E. Pavarini, A. Yamasaki, J. Nuss, and O. K. Andersen, cond-mat/0504034.
- 54 T. Mizokawa and A. Fujimori, Phys. Rev. B 54, 5368 (1996).
- 55 For  $\text{SrVO}_3$  we have obtained  $W_{t_{2g}} = 2.3 \text{ eV}$ , while Pavarini et al. reported  $W_{t_{2g}} = 2.9 \text{ eV}$ .<sup>53</sup> The electronic structure of cubic

perovskites has been systematically studied by K. Takegahara [J. Electron Spectrosc. Relat. Phenom. 66, 303 (1994)], using the augmented plane wave method within  $m$ - $n$ - $t$ in approximation. For  $\text{SrVO}_3$ , he had  $W_{t_{2g}} = 2.4$  eV. This electronic structure has been used in DMFT calculations by A. Liebsch [Phys. Rev. Lett. 90, 096401 (2003)]. There is another cubic perovskite,  $\text{SrTiO}_3$ , which has been intensively investigated by first-principle electronic structure calculations. For this material, the full-potential calculations yield  $W_{t_{2g}} = 2.5$  eV [e.g., S. Kimura et al., Phys. Rev. B 51, 11049 (1995)], which is in fair agreement with our finding  $W_{t_{2g}} = 2.4$  eV. Takegahara's value is  $W_{t_{2g}} = 2.5$  eV. The orthorhombic  $\text{YTiO}_3$  has been studied in details by H. Sawada and K. Terakura [Phys. Rev. B 58, 6831 (1998)]. They have obtained  $W_{t_{2g}} = 1.7$  eV. It is important to note that this value corresponds to the generalized gradient approximation (GGA), which additionally splits the  $t_{2g}$ -bands because of strong nonsphericity of the exchange-correlation potential. This nonsphericity should be suppressed in the process of construction of the Hubbard Hamiltonian (see Sec. V). Therefore, our value  $W_{t_{2g}} = 1.5$  eV for  $\text{YTiO}_3$  seems to be reasonable. On the other hand, Pavarini et al. reported (using the atomic-spheres approximation, similar to ours)  $W_{t_{2g}} = 2.05$ , which was even larger than the  $t_{2g}$ -bandwidth of the considerably less distorted  $\text{LaTiO}_3$ . Also, for  $\text{LaTiO}_3$  we did not observe any overlap between  $\text{Ti}(t_{2g})$  and  $\text{La}(5d)$  bands, reported in Ref. 53.